

AD-A100 128

CALIFORNIA UNIV BERKELEY DEPT OF PHYSICS
CONVERSION GAIN IN MM-WAVE QUASIPARTICLE HETERODYNE MIXERS, (U)

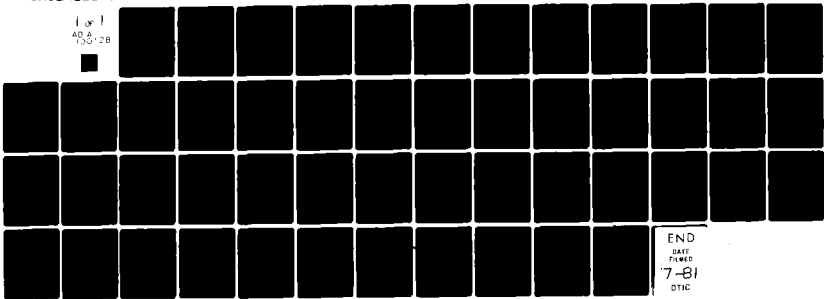
1981 T M SHEN

F/6 9/4

NL

UNCLASSIFIED

For I
AD 6-2B
[Redacted]



END
DATE
FILED
7-81
DTIC

IEEE Journal Of Quantum Electronics, July 1981 (To be published)

CONVERSION GAIN IN MM-WAVE
QUASIPARTICLE HETERODYNE MIXERS

T. M. SHEN

Department of Physics
University of California
Berkeley, California 94720

REF ID: A6512

ABSTRACT

100-51

The physical mechanisms which give rise to conversion gain in SIS quasiparticle mixers are studied. It is shown that the S-shape tunneling structure at the gap voltage of the I-V curve is essential in achieving conversion gain. In the development of SIS quasiparticle mixers, a new approach is used to analyse the embedding network of the mixing experiment. This method as described in this paper has the advantage over conventional methods that no separate measurements are necessary. In order to obtain a complete picture of the performance of SIS quasiparticle mixers, the photon-assisted tunneling theory used by Tucker to describe quasiparticle mixing is extended here to include pair current contribution. Based on this complete quantum theory the effects of the Josephson noise on SIS quasiparticle mixing is discussed and an upper frequency limit of SIS quasiparticle mixing is estimated.



AD A100128

100-51 COPY

* Present Address: Bell Laboratories, 600 Mountain Ave., Murray Hill, New Jersey 07974

81 6 12 012

CONVERSION GAIN IN MM-WAVE QUASIPARTICLE HETERODYNE MIXERS

T. M. Shen*

Department of Physics
University of California
Berkeley, California 94720

I. INTRODUCTION

Applications such as radioastronomy have stimulated development of low noise receivers for millimeter and submillimeter wavelength electromagnetic radiation. Superconducting tunnel junctions have long been considered as possible nonlinear elements for low noise receivers in this wavelength range. The properties of Josephson effect detectors and mixers have been investigated by many workers but they have not been actively used as their performance is limited by intrinsic noise due to down-conversion of high frequency noise by Josephson effects. Recently attention has focused on making use of the nonlinearity of quasiparticle tunnel junctions for millimeter and submillimeter wave detection and mixing. Some of these devices now appear competitive for low noise applications. The first type of quasiparticle junction to be used for detection and mixing experiments was the super-Schottky diode [1-3]. This is a superconductor — semiconductor tunneling structure. The current-voltage (I-V) curves of these super-Schottky diodes are essentially the same as those of superconductor-insulator-normal metal (SIN) tunnel junctions. The Schottky barrier created on the surface of the semiconductor provides the tunneling barrier. At temperatures less than the superconducting transition temperature T_c , thermionic emission over the barrier can be neglected and the diode current is dominated by quasiparticle tunneling. Superconductor-insulator-normal metal SIN junctions could also be used for quasiparticle devices, but have not been widely explored. Recent device work is focusing on superconductor-insulating oxide-superconductor SIS (Josephson) tunnel junctions [4-14]. Due to the singularity in density of states of quasiparticles in the superconductors on two sides of the oxide barrier, there is a sudden onset of quasiparticle tunneling current at bias voltage near the full superconducting gap voltage $2\Delta/e$. The quasiparticle tunneling

current is hence highly nonlinear near the gap voltage. Pair (Josephson) tunneling current provides another conducting path for SIS junctions. When an SIS device is operated in the quasiparticle mode, it is biased near the superconducting gap voltage $2\Delta/e$. If the junction capacitance is sufficiently large the junction will be shorted at the Josephson frequency and Josephson effects can be neglected.

The theory of quasiparticle tunneling has been studied extensively. In a recently published paper, Tucker [4] has given a complete review of those aspects of the photon-assisted quasiparticle tunneling theory which are relevant for detection and mixing. Results of his general quantum mixer theory indicate that, at frequencies where the photon energy exceeds the range of the dc nonlinearity on the I-V curve on the voltage scale, classical theory breaks down and photon-assisted tunneling theory must be used to understand device performance. The theory shows that the response of the quasiparticle tunneling currents to an RF drive at frequency ω is dominated by quantum effects when the voltage range of the nonlinearity of the I-V curve is less than $\hbar\omega/e$. Theoretical analysis of ideal SIN and SIS junctions predicts that at sufficiently low temperature both of these devices will display quantum effects at millimeter wave and sub-millimeter wave frequencies. Quasiparticle mixing up to 30 GHz using super-Schottky diodes operated at 1K has been reported [3]. In these experiments, the super-Schottky diodes were operated in the classical limit with conversion efficiency less than unity. Problems associated with coupling and parasitic losses have prevented super-Schottky devices from being operated at higher frequencies at which quantum effects might be seen. In SIS junctions the non-linearity of the I-V curve is confined to a narrower range of voltage than in SIN junctions. At temperatures well below the superconducting transition temperature T_c , series resistance in SIS junctions is negligible. As a consequence SIS junctions are capable of displaying strong quantum effects even in the millimeter wave frequency range [5-8]. In particular, conversion gain in SIS mixers operated in the quantum limit was theoretically predicted [9] and was experimentally observed [6] at 36 GHz with a mixer noise temperature approaching the quantum limited value of $T_M \approx \hbar\omega/k$. SIS quasiparticle mixers have been developed very rapidly in the past two years and have been demonstrated to be attractive devices for low noise detection in millimeter and

submillimeter wave radiation. A detailed description of the development of SIS devices can be found in a recent review article [10] by Richards and Shen. During this period of development new theories and techniques have been evolved in order to understand the physics and performance of this device. At temperature well below T_c , SIS tunnel junctions have negligible series resistance. Therefore, as will be shown, there is good reason to expect that SIS quasiparticle mixers can operate at frequencies approaching the full superconducting gap frequency (which has a value of $2\Delta/h \sim 800$ GHz for Pb). At these high frequencies the Josephson effects will become significant. In this paper the theory of SIS quasiparticle mixing is extended to include the effects arising from the pair tunneling currents.

The properties of frequency conversion in nonlinear devices have been analyzed in detail by many authors [15-20]. The small-signal performance of a periodically pumped nonlinear device is usually described by an admittance matrix whose matrix elements are complicated functions of the properties of the device and the operating conditions. Quantum effects have been omitted in determining these matrix elements in classical mixer analysis [21-27]. For an SIS mixer operating in the quantum limit these classical expressions are no longer applicable and photon-assisted tunneling theory must be used to evaluate the matrix elements. The classical prohibition of conversion gain in resistive mixers is removed. In Section II the analysis of general nonlinear devices is summarized. The general expression for conversion loss is rewritten in a compact form which is particularly suitable for computer calculations. In Section III it will be shown that the S-shape tunneling structure on the I-V curves of SIS junctions is essential for achieving conversion gain. Since the results of photon-assisted tunneling theory indicates that there exists a nonlinear quantum susceptive element [4] its contribution to frequency conversion cannot be neglected. The role played by this nonlinear quantum susceptive term in the observed conversion gain [6] will be discussed.

In order to understand fully the performance of a device in a mixing experiment, a theoretical calculation in connection with a mixing experiment is desirable. A problem one soon encounters is the determination of the admittance in the embedding network. The complicated geometry of waveguide mounting structure makes theoretical evaluation [28] difficult. Previous

approaches have used admittance measurements on scale models [29] at much lower frequencies than the actual signal frequency, or by reflectometer methods [30] in which reflectivities are measured in separate measurements. During the course of development of SIS devices, a new approach [6,11] was used to determine the admittance of the embedding network. This method extracts the information about the admittance of the embedding network from the response of the dc I-V curve to external radiation obtained in the mixing experiment. No separate measurements are involved. This is clearly an advantage over conventional methods. An application of this method to computer simulation of an SIS mixing experiment will be illustrated in Section IV.

The present quantum mixing theory of SIS mixers only includes contributions from quasiparticle tunneling current, pair tunneling effects having been neglected. This approximation remains valid as long as the junction capacitance is sufficiently large to short out the junction at the Josephson frequencies. The I-V curve of small area junctions suitable for mixing at 115 GHz [12] already contained a significant contribution from pair tunneling. At higher frequencies pair tunneling effects can no longer be neglected. In Section V of this paper a complete quantum mixing theory is presented. The formalism of photon-assisted tunneling theory used by Tucker to describe quasiparticle mixing is extended to include contributions from pair tunneling effects. This theory gives a complete picture of the performance of SIS mixer and is essential for the future development of SIS devices. Based on this theory the effects of Josephson noise on SIS quasiparticle mixing is discussed in Section VI and an upper frequency limit of SIS quasiparticle mixers is estimated.

II. GENERALIZED MIXER ANALYSIS

The basic principles of frequency conversion using nonlinear devices have been dealt in depth by many authors [4,15-20]. The results of the analysis are summarized in this section. The general expression for the conversion loss of any nonlinear device is rewritten in a compact form which is particularly suitable for computer calculations.

We will follow the notations as used in reference [4]. The equivalent circuit for a general nonlinear mixer can be represented by a Y-mixer model as illustrated in Fig. 1. An applied local oscillator at frequency ω mixes with all side-band frequencies

$$\omega_m = m\omega + \omega_0, \quad m = 0, \pm 1, \pm 2, \dots \quad (2.1)$$

to give an output at ω_0 . Each sideband is assumed to be terminated by an admittance Y_m . Power is down-converted from the signal frequency $\omega_S = \omega_1$ with a current generator I_S and source admittance $Y_S = Y_1$ to the intermediate frequency (IF) $\omega_{IF} = \omega_0$ with a load $Y_L = Y_0$.

The small-signal current and voltage at various sidebands are interrelated by an admittance matrix $Y_{mm'}$ (hence called the Y-mixer model),

$$i_m = \sum_{m'} Y_{mm'} v_{m'} \quad (2.2)$$

The elements of this admittance matrix depend heavily on the nonlinearities of the device, the impressed local oscillator waveform across the diode, the dc bias and the frequencies of operation. This small-signal voltage response can be related to the set of current generators I_m by

$$I_m = i_m + Y_m v_m \quad (2.3)$$

Combining Eqs. (2.2) and (2.3) we have

$$I_m = \sum_{m'} Y'_{mm'} v_{m'} \quad (2.4)$$

where the augmented matrix $Y'_{mm'}$ is given by

$$Y'_{mm'} = Y_{mm'} + Y_m \delta_{mm'} \quad (2.5)$$

Inverting this relation we get

$$v_m = \sum_{m'} Z_{mm'} I_{m'} \quad (2.6)$$

where the matrix

$$||Z_{mm'}|| = ||Y'_{mm'}||^{-1} \quad (2.7)$$

The conversion loss of a mixer is defined as

$$L = \frac{\text{Power available at the signal frequency } \omega_1}{\text{Power delivered to the load at IF frequency } \omega_0}$$

$$= \frac{1}{4G_S G_L |Z_{01}|^2}, \quad (2.8)$$

where G_S and G_L represent the real parts of the source and load admittance Y_S and Y_L , respectively. Expression (2.8) is presented as Eq. (7.7) in reference [4]. We will proceed to separate out from (2.8) a conversion loss factor associated with the nonlinear element and an IF mismatch factor. The matrix element Z_{01} can be written as

$$Z_{01} = \frac{Cf_{10}}{\det}, \quad (2.9)$$

where Cf_{10} and \det denote the cofactor and determinant of the augmented matrix $||Y'_{mm}||$. If we further define \det' as the determinant of the augmented matrix $Y'_{mm'}$ with $Y_L = 0$,

$$\det' = \text{determinant of } ||Y'_{mm'}||_{Y_L=0}, \quad (2.10)$$

then Eq. (2.8) can be written as

$$L = \frac{1}{4G_S G_L} \frac{|\det|^2}{|Cf_{10}|^2}$$

$$= \frac{1}{4G_S G_L} \frac{|\det' + Y_L \cdot Cf_{00}|^2}{|Cf_{10}|^2}$$

$$= \frac{G_{IF}}{G_S} \cdot \frac{|Cf_{00}|^2}{|Cf_{10}|^2} \cdot \frac{|Y_{IF} + Y_L|^2}{4G_{IF} G_L}$$

$$= L^0 \cdot \frac{1}{C_{IF}}, \quad (2.11)$$

where

$$Y_{IF} = \frac{\det'}{Cf_{00}} = G_{IF} + jB_{IF}, \quad (2.12)$$

$$\frac{1}{C_{IF}} = \frac{|Y_{IF} + Y_L|^2}{4G_{IF}G_L}, \quad (2.13)$$

$$L^0 = \frac{G_{IF}}{G_S} \cdot \frac{|Cf_{00}|^2}{|Cf_{10}|^2}. \quad (2.14)$$

Here Cf_{00} and Cf_{10} are cofactors of the augmented matrix $\begin{vmatrix} Y_{mm} & Y_{ml} \\ Y_{lm} & Y_{ll} \end{vmatrix}$. C_{IF} represents the IF coupling factor at the output with an IF admittance Y_{IF} given by Eq. (2.12). Expressions (2.11) to (2.14) are valid for any N-port nonlinear devices without parasitic losses. These compact forms are particularly suitable for computer calculations. Expressions (2.11) to (2.14) can be shown to reduce to the conventional expressions for special cases such as nonlinear resistive diodes [4,15,16], two-port parametric amplifiers [18] and double-side-band parametric down-converters [31].

From expressions (2.11) to (2.14) we can see that matched condition is achieved at the output with a load

$$Y_L = G_L + jB_L, \quad (2.15)$$

with

$$G_L = |G_{IF}| \text{ and } B_L = -B_{IF}. \quad (2.16)$$

There are two possible cases. In the first case where

$$G_{IF} = \operatorname{Re} Y_{IF} > 0, \quad (2.17)$$

then under matched condition (2.16),

$$\frac{1}{C_{IF}} = 1, \quad (2.18)$$

and

$$L = L^0 \cdot \frac{1}{C_{IF}} \\ = \frac{G_{IF}}{G_S} \left| \frac{Cf_{00}}{Cf_{10}} \right|^2. \quad (2.19)$$

Conversion gain with positive IF conductance is possible when L^0 is less than unity. In the second case where

$$G_{IF} = \text{Re } Y_{IF} \leq 0, \quad (2.20)$$

then under the matched condition (2.16)

$$\frac{1}{C_{IF}} = 0 \quad (2.21)$$

and

$$L = L^0 \cdot \frac{1}{C_{IF}} = 0. \quad (2.22)$$

Infinite gain can be achieved from the negative IF conductance. Note that a negative IF conductance G_{IF} is accompanied by a negative value of L^0 .

For mixer analysis, a lot of information can be obtained by examining the value of L^0 expressed in Eq. (2.14). A positive value of L^0 indicates that G_{IF} is positive and the minimum conversion loss L under matched condition is L^0 . Conversion gain is possible whenever L^0 has a value less than unity. On the other hand, a negative value of L^0 indicates that G_{IF} is negative. Although unlimited gain ($L = 0$) is possible in the matched condition, such a bias condition may not be suitable for mixer operation as it would easily break into oscillation. In the discussion of conversion gain in the next section, we will assume the device is matched at the output and conversion loss L^0 will be calculated.

III. CONVERSION GAIN IN SIS AND SIN QUASIPARTICLE MIXERS

In this section we will examine the conversion gain in SIS and SIN quasiparticle mixers. We will first examine the role played by the nonlinear quantum reactance in the power conversion. We shall see that the contribution from the nonlinear quantum reactance can be relatively

insignificant and conversion gain can be basically accomplished by the nonlinear conductive term. We will then show that the S-shape tunneling structures at the gap voltage in SIS and SIN junctions are essential in achieving conversion gain.

The performance of SIS and SIN quasiparticle mixers are completely characterized by the complex response function $j_1(\omega)$ [4,34,35]. Closed form expressions for these complex response functions in quasiparticle tunnel junctions at low temperatures $kT \ll \Delta$ were obtained by Werthamer [34] and analyzed by Harris [35]. For SIS junctions with identical superconductors the idealized quasiparticle response function takes the form

$$[\text{Im } j_1(\omega)]_{T=0} = \begin{cases} 0 & 0 \leq x \leq 1 \\ G_N \frac{2\Delta}{e} \left[xE(1-\frac{1}{x^2}) - \frac{1}{2x}K(1-\frac{1}{x^2}) \right] & 1 \leq x < \infty \end{cases} \quad (3.1)$$

$$[\text{Re } j_1(\omega)]_{T=0} = \begin{cases} G_N \frac{2\Delta}{e} \left[\frac{1}{2}K(x^2) - E(x^2) + \frac{\pi}{4} \right] & 0 \leq x \leq 1 \\ G_N \frac{2\Delta}{e} \left[x[K(\frac{1}{x^2}) - E(\frac{1}{x^2})] - \frac{1}{2x}K(\frac{1}{x^2}) + \frac{\pi}{4} \right] & 1 \leq x < \infty \end{cases} \quad (3.2)$$

Here K and E are complete elliptic integrals of first and second kind with the parameter m given by the arguments of the elliptic integrals and $x = \hbar\omega/2\Delta$. G_N is the normal state junction conductance at high voltages. For an SIN junction the idealized quasiparticle response function is given by

$$[\text{Im } j_1(\omega)]_{T=0} = \begin{cases} 0 & 0 \leq x \leq 0.5 \\ G_N \frac{\Delta}{e} [(2x)^2 - 1]^{\frac{1}{2}} & 0.5 \leq x < \infty \end{cases} \quad (3.3)$$

$$[\text{Re } j_1(\omega)]_{T=0} = \begin{cases} G_N \frac{\Delta}{e} \left[1 - \sqrt{1 - (2x)^2} \right] & 0 \leq x \leq 0.5 \\ G_N \frac{\Delta}{e} & 0.5 \leq x < \infty \end{cases} \quad (3.4)$$

In these expressions the imaginary parts of the response functions give the corresponding dc I-

V characteristics of the junctions. The nonlinear quantum susceptive element arises from the real part of the response function $j_1(\omega)$ which is related to the imaginary parts of the response function through the Kramers-Kronig transform [4,34,35]. These response functions are shown in Figs. 2 and 3.

In order to understand the relative importance of the nonlinear quantum susceptive term compared with the nonlinear quantum conductive term we will examine the role played by the nonlinear quantum susceptance in the conversion gain for a particular SIS quasiparticle mixer [6]. The mixing experiment is carefully analyzed using the 3-port (signal, image and IF) Y-mixer model and the method described in the next section. The impressed local oscillator waveform and the source admittance ($0.07-j 0.007$) Ω^{-1} are deduced by fitting to the dc I-V curve under applied local oscillator power. This information is then used in the computer calculation of the 3-port Y-mixer network to simulate the mixing experiment. The local oscillator voltage is assumed to be purely sinusoidal. In this particular case, the contributions from the nonlinear conductance $Im j_1(\omega)$ and the quantum susceptance $Re j_1(\omega)$ are represented by the real part and imaginary part of the admittance matrix element $G_{mm}+jB_{mm}$, respectively. Results of the calculation are shown in Table 1. The double-side-band (DSB) conversion efficiencies with the bias point at the first four photon peaks from the gap voltage $2\Delta/e$ are calculated. The first column shows the calculated conversion efficiency using the full quantum admittance matrix elements $G_{mm}+jB_{mm}$. In order to examine the role played by the nonlinear quantum susceptance B_{mm} , the conversion efficiency is recalculated using only the nonlinear conductive term G_{mm} . The result is shown in the second column. The contribution from the nonlinear quantum susceptive term is examined by taking the ratio (shown in the third column) of the conversion efficiency in the first column to that in the second column. We see that except with a bias point at the first photon peak the contribution from the nonlinear quantum susceptance is relatively insignificant. In particular, with a bias point at the fourth photon peak at which conversion gain was observed experimentally, the conversion gain is basically accomplished by the nonlinear conductive element. The nonlinear quantum susceptive term only contributes about 2% to the total power output at the IF frequency. Although at the first photon peak the

calculated conversion efficiency which includes the contribution from the quantum susceptance is about 3.20 larger, it is pointed out by Feldman [37] that the significance of the quantum susceptance should not be overemphasized by comparing these calculated values at one bias point. When the junction is biased near the gap voltage the conversion efficiency is very sensitive to all the parameters. A thorough exploration of the parameter space in this region indicates that a large conversion gain can also be obtained from the nonlinear conductive term by slightly changing the bias conditions [37]. Another analytical approach is to calculate the conversion efficiency using the 3-port Y-mixer model in the limit of small $\alpha = eV_1/\hbar\omega$, where V_1 is the local oscillator voltage at frequency ω . The result indicates that in this limit the contribution from the nonlinear quantum susceptance is relatively insignificant when compared with that from the nonlinear conductive term [37]. At the same time, the results of computer calculations [13] show that the favorable conditions for achieving conversion gain mostly occur in this limit of small α . This shows that the nonlinear conductive term plays a more important role in achieving conversion gain in SIS quasiparticle mixers.

We will now show how conversion gain can be accomplished by the nonlinear conductive element through the S-shape tunneling structures at the gap voltage in SIS and SIN junctions. Since the quantum susceptance is not essential in achieving the conversion gain in SIS quasiparticle mixers its contribution will be neglected in this discussion. Consider a 3-port Y-mixer model with the limit of zero IF frequency. The local oscillator voltage can be assumed to be sinusoidal. In this case Eq. (2.14) gives a single sideband (SSB) conversion loss of

$$L^0 = 2 \frac{G_{10}}{G_{01}} \cdot \frac{(y_s + 1)(y_s + 1 - \eta)}{y_s \eta} , \quad (3.5)$$

where

$$y_s = G_S/G_{11} , \quad (3.6)$$

$$\eta = \frac{2G_{10}G_{01}}{G_{00}(G_{11} + G_{1-1})} . \quad (3.7)$$

The dependence of L^0 on y_s in Eq. (3.5) is shown in Fig. 4. When $\eta > 1$, L^0 becomes negative

for $y_s < \eta - 1$. The IF conductance is negative and unlimited gain is possible. When $\eta < 1$, L^0 is positive for all values of y_s and attains its minimum value of

$$L_{\min}^0 = 2 \frac{G_{10}}{G_{01}} \cdot \frac{1 + \sqrt{1-\eta}}{1 - \sqrt{1-\eta}}. \quad (3.8)$$

at a value of $y_s = \sqrt{1-\eta}$ [4,15,16]. The IF conductance is positive and stable operation is possible. As η approaches 1, L_{\min}^0 approaches to $2G_{10}/G_{01}$, which could be less than 2 if G_{10}/G_{01} is less than unity. In classical theory the conductance waveform $g(t)$ as a function of time (and hence the conductance matrix element) is obtained by taking the derivatives on the I-V curve and a minimum SSB conversion loss of greater than 2 is predicted. When SIS quasiparticle mixers are operated in the quantum limit, the conductance waveform $g(t)$ is no longer given by the derivatives on the I-V curve and photon-assisted tunneling theory must be used to obtain the admittance matrix elements. From Eq. (7.21) of reference [4], we have in the limit of zero IF frequency,

$$G_{10} = \sum_n J_n(\alpha) J_{n+1}(\alpha) \cdot \frac{1}{2} \cdot \left[\frac{dI_{dc}}{dV} (V_0 + (n+1) \frac{\hbar\omega}{e}) + \frac{dI_{dc}}{dV} (V_0 + n \frac{\hbar\omega}{e}) \right], \quad (3.9)$$

$$G_{01} = \sum_n J_n(\alpha) J_{n+1}(\alpha) \left[I_{dc}(V_0 + (n+1) \frac{\hbar\omega}{e}) - I_{dc}(V_0 + n \frac{\hbar\omega}{e}) \right] \sqrt{\frac{\hbar\omega}{e}}. \quad (3.10)$$

$J_n(\alpha)$ is the Bessel function of order n with argument $\alpha = \frac{eV_1}{\hbar\omega}$, where V_1 is the local oscillator voltage of frequency ω . In quantum theory the matrix element G_{nm} depends on the points on the I-V curve separated by $\hbar\omega/e$. For convenience we refer to these points as "photon points". The transfer matrix element G_{10} for an IF photon depends on the derivatives of the I-V curve because in the limit $\omega_0 = 0$, the IF conductance is given by the derivatives on the I-V curve as in the classical theory. The transfer matrix element G_{01} for a signal photon depends on the

conducting chord joining the "photon points" on the I-V curve. Of course, these terms are equal for a linear device. For a nonlinear I-V curve arising from a tunneling diode such as the SIS device shown in Fig. 2 the range of nonlinearity is much smaller than the photon energy on the voltage scale. In the vicinity of the gap structure at $2\Delta/e$, where there is a sudden jump in tunneling current, the derivatives of the I-V curve at the "photon points" A and B are much smaller than the conductance of the chord joining A and B. Hence, under proper bias conditions, G_{10} can be much smaller than G_{01} and conversion gain may be achieved. A similar argument can be applied to the case of SIN quasiparticle mixers to show that conversion gain is possible under proper bias conditions near the gap voltage Δ/e . Due to the absence of a jump in the tunneling current the conversion gain effect in SIN junctions is expected to be less pronounced than in SIS junctions.

Computer simulations on the performance of quasiparticle mixers in SIS and SIN junctions have been performed. Results of the computer simulations are reported in the recent work by Shen and Richards [13]. Conversion gain in quasiparticle mixers in SIS and SIN junctions is predicted over a wide range of experimental parameters.

IV. COMPUTER ANALYSIS OF MIXING EXPERIMENT

A problem that is often encountered at microwave and millimeter wave frequencies is the determination of the admittances in an embedding network for various devices mounted in actual circuits such as mixer diodes. A theoretical evaluation [28] of the admittance parameters of this network is usually very difficult due to the often very complicated geometry of practical mounting structures. Several methods of dealing with the problem of measuring the elements of embedding networks have been used. For millimeter wave mixers the usual approach has been to use admittance measurements made on scale models at much lower frequency than the actual signal frequency [29]. Although valuable information can be obtained in this way, this technique is time consuming and tedious and has some inherent difficulties. Structures like electrical leads which are not negligibly small are very difficult to be taken into account in large-scale modeling. It is known that the admittance elements in the embedding network is

very sensitive to the way the junctions are mounted. Hence the measured admittance elements may not give the correct value of the embedding admittance for different mixing experiments. Another way to determine the admittances of the embedding network is by reflectometer method [30]. Its accuracy depends on the directivity of the directional coupler used and also on the power level of the test signal. Once the embedding admittances are determined the local oscillator waveform is obtained by solving the circuit equations self-consistently [36].

In the research on SIS quasiparticle mixers, a new approach [6,11,13] has been used to analyze the experiment. The information of the admittances of the embedding network is deduced from the dc I-V curve under external radiation in the *actual* experiment; no separate measurement is necessary. Hence the admittance elements obtained are those in the embedding network of the actual experiment. This eliminates the problem of representing the actual experimental circuitry that is faced in theoretical analysis, large scale modeling and reflectometer measurement. This method is exceptionally simple in the case of the SIS quasiparticle mixer where the junction capacitance is voltage independent and the series resistance is negligible. With slight modification this method can be extended to include effects such as voltage dependent junction capacitance and frequency dependent series resistance in the case of SIN quasiparticle mixers.

The principle behind this method is to extract the informations about the embedding admittances at the local oscillator frequency and its harmonics from the dc current response of the junction under local oscillator drive. Since the embedding admittance at the various frequencies will affect the local oscillator voltage waveform impressed acrossed the junction, the dc current response will also depend on the admittance elements in the embedding network. The impressed local oscillator waveform can be deduced by fitting the theoretical dc I-V curve to the experimental curve, and the admittance elements of the embedding network can be determined from the circuit equations. It is convenient to consider the junction capacitance as part of the embedding admittance.

The mixer analysis is based on the experimental measured I-V curve which is taken to be

the imaginary part of the quasiparticle response function j_1 . The corresponding real part of the response function is deduced from the requirement of causality by using the numerical Kramers-Kronig transform.

Under a local oscillator drive,

$$V_{L0}(t) = \sum_{m=-\infty}^{\infty} V_m e^{im\omega t}, \quad (4.1)$$

the time dependent quasiparticle tunnel current from photon-assisted tunneling theory [4] is

$$I(t) = \text{Im} \sum_{m,n=-\infty}^{\infty} \frac{W(n\omega)W^*((n+m)\omega)}{xj_1(n\omega + \frac{eV_0}{\hbar}) e^{im\omega t}} \quad (4.2)$$

$$= \sum_{m=-\infty}^{\infty} I_m e^{im\omega t}, \quad (4.3)$$

In Eq. (4.2), the coefficient $W(\omega)$ is given by the Fourier transform.

$$\int_{-\infty}^{\infty} d\omega W(\omega) e^{-i\omega t} = \exp \left[-\frac{ie}{\hbar} \int_0^t dt' V_{L0}(t') \right]. \quad (4.4)$$

The voltage amplitude V_m across the junction are adjusted until the dc current I_0 computed from Eq. (4.2) agrees with the measured dc I-V curves under constant local oscillator power at all dc bias voltage. The embedding admittances Y_m at various frequency ports can then be calculated from the circuit equations,

$$I_p = V_1 Y_1 + I_1 \quad (4.5)$$

$$0 = V_m Y_m + I_m \quad m \neq 1 \quad (4.6)$$

Here I_p is the current source amplitude at the local oscillator frequency. Once V_m 's are determined through the fitting to the experimental dc I-V curve, all the ac currents I_m can be calculated from Eqs. (4.1) to (4.4). The embedding admittance Y_m can then be determined from Eqs. (4.5) and (4.6). Note that the ordered pair (V_m, I_m) is a function of the dc bias V_0 . A change in V_0 will effectively change the admittance of the junction and hence its voltage and

current. Consequently, all the Y_m 's determined from Eqs. (4.5) and (4.6) have to satisfy these equations at *all* dc bias voltages. The whole problem has to be solved in a self-consistent manner. Note that in this method the embedding admittance *and* the local oscillator waveform are both determined through the iterations.

In practical fundamental mixers, attempts are made to prevent power dissipation at harmonic sideband frequencies. The 3-port Y-mixer model is often used to analyze the experimental data. This 3-port Y-mixer model is a useful approximation to SIS mixers as the junction capacitance provides the necessary high admittance termination at harmonic frequencies. Even in a 3-port model, the conversion loss is a complicated function of the dc bias V_0 , local oscillator drive V_1 , signal frequency ω_S , IF frequency ω_{IF} , RF source admittance $G_S + jB_S$ and IF load admittance $G_L + jB_L$. In analyzing an experimental situation the frequencies of operation ω_S and ω_{IF} , ($\omega_{IF} \ll \omega_S$) and the IF load admittance $G_L + jB_L$ are known. The dc bias voltage V_0 is a measurable quantity. The local oscillator voltage is changed by adjusting the available local oscillator power which is a measurable quantity. The source admittance $G_S + jB_S$ is adjusted by tuning the stub and plunger which form the microwave coupling cavity, but the values of G_S and B_S are still unknown. Within the context of a 3-port Y-mixer model the problem remaining is to determine the local oscillator waveform impressed across the diode and the source admittance at the local oscillator frequency.

When a 3-port Y-mixer model is used, the computation required to obtain a self-consistent solution from Eqs. (4.1) to (4.6) is much reduced because it is now sufficient to consider only the frequencies corresponding to $m=1, 0$ and -1 . In particular, the local oscillator voltage waveform impressed across the junction given by Eq. (4.1) reduces to

$$V_{LO}(t) \approx V_1 e^{i\omega t}. \quad (4.7)$$

Without loss of generality we may choose V_1 to be real. In this case, the Fourier coefficient $W(n\omega)$ expressed in Eq. (4.4) takes the form of $J_n(\alpha)$, Bessel function of order n and argument $\alpha = eV_1/n\omega$ [4]. From Eq. (4.2) the dc current at the voltage V_0 under a local oscillation drive of $V_1 \cos(\omega t)$ is given by,

$$I_0(V_0) = \sum_{n=-\infty}^{\infty} |J_n(\alpha)|^2 I_{dc}(V_0 + n \frac{\hbar\omega}{e}) . \quad (4.8)$$

For each bias point V_0 , V_1 is varied until the dc current calculated from Eq. (4.8) agrees with the measured dc current at the bias voltage V_0 . In this way the local oscillator voltage waveform at all bias point can be determined. To determine the local oscillator source admittance as seen by the diode, let us consider the equivalent circuit at the local oscillator frequency ω as shown in Fig. 5. I_p is the current amplitude of the local oscillator drive and $G_S + jB_S$ represents the source admittance referred to the reference plane of the junction. The junction capacitance (being voltage independent in the case SIS junctions) is considered as part of the source admittance. From (4.2) the component of the tunneling current at the local oscillator frequency ω is given by

$$I_1 e^{i\omega t} = \text{Im} \sum_{n=-\infty}^{\infty} J_n(\alpha) J_{n+1}(\alpha) j_1(n\omega + \frac{eV_0}{\hbar}) e^{i\omega t} . \quad (4.9)$$

The amplitude of the current source is

$$I_p = V_1(G_S + jB_S) + I_1 . \quad (4.10)$$

The available power from the local oscillator is

$$\begin{aligned} P_{LO} &= \frac{1}{8G_S} |I_p|^2 \\ &= \frac{1}{8G_S} \{(V_1 G_S + R e I_1)^2 + (V_1 B_S + I_m I_1)^2\} . \end{aligned} \quad (4.11)$$

Equation (4.11) can be rearranged to give the equation of a circle:

$$(G_S - x_0)^2 + (B_S - y_0)^2 = r^2 , \quad (4.12)$$

with radius

$$r = \left[\left(\frac{4P_{LO}}{V_1^2} - \frac{R e I_1}{V_1} \right)^2 - \left(\frac{R e I_1}{V_1} \right)^2 \right]^{\frac{1}{2}} . \quad (4.13)$$

and centered at

$$x_0 = \frac{4P_{LO}}{V_1^2} - \frac{Re I_1}{V_1}, \quad (4.14)$$

$$y_0 = -\frac{Im I_1}{V_1}. \quad (4.15)$$

Hence the source conductance G_S and susceptance B_S are constrained to lie on a circle centered at (x_0, y_0) with a radius r given by Eq. (4.13), (4.14) and (4.15). The values of x_0 , y_0 and r not only depend on P_{LO} explicitly, but also on the dc bias V_0 implicitly through V_1 and I_1 . Different pairs of values of P_{LO} and V_0 will then give different circular loci. For one dc bias point V_0 , such a circle C_1 is obtained as illustrated in Fig. 6. By repeating the process for other points V_0 on the I-V curve, and/or with different local oscillator power a number of circles such as C_2 and C_3 in Fig. 6 can be drawn. Within the validity of the 3-port model, all these circles should intersect at a point (G_S, B_S) which is the conductance and susceptance of the current source as seen by the junction. In this way the source admittance and the impressed local oscillator waveform at all dc bias voltage V_0 under constant local oscillator power can be determined. Once the embedding admittance and the impressed local oscillator waveform are determined, conversion loss and other properties of the mixer can be calculated in a manner similar to classical mixer analysis [17,20] except that classical expressions have to be replaced by quantum expressions where appropriate. Figure 7 shows an experimental I-V curve for an SIS junction with the corresponding theoretical curve computed using the local oscillator waveform and source admittance determined in this way in a 3-port model. Agreement is excellent, considering that higher harmonics have not been considered.

When the circular loci of the source admittance fail badly to intersect at one point, this is an indication of inadequacy of the 3-port model. The 5-port Y-mixer model which includes the first harmonics of the local oscillator frequency can then be used. In this case, we have to consider a local oscillator voltage of the form

$$V_{LO}(t) = V_1 e^{i\omega t} + V_2 e^{i2\omega t}. \quad (4.16)$$

Here V_1 can be chosen to be real but V_2 in general is complex. The coefficient $W(n\omega)$ given by

Eq. (4.4) no longer takes a simple form of a Bessel function but can still be easily evaluated on a computer by taking the product of three Bessel series. Due to the phase dependence in V_2 , $W(n\omega)$ is complex and takes the form,

$$W(n\omega) = \sum_{n=-\infty}^{\infty} \sum_{k=-\infty}^{\infty} \left[(-1)^k J_{n-2k-4k}(\alpha) J_n(\beta) J_{2k}(\beta') + i(-1)^k J_{n-2k-4k+2}(\alpha) J_n(\beta) J_{2k-1}(\beta') \right], \quad (4.17)$$

where

$$\alpha = \frac{eV_1}{\hbar\omega}, \beta = \frac{eRcV_2}{2\hbar\omega} \text{ and } \beta' = \frac{elmV_2}{2\hbar\omega}. \quad (4.18)$$

V_2 may be determined through a second order fitting to the measured dc I-V curve. Once V_1 and V_2 are determined the current at the harmonic frequency 2ω can be calculated from

$$I_2 e^{i2\omega t} = \text{Im} \sum_{n=-\infty}^{\infty} W(n\omega) W^*((n+2)\omega) j_1(n\omega + \frac{eV_0}{\hbar}) e^{i2\omega t}. \quad (4.19)$$

The admittance $G_2 + jB_2$ at the harmonic frequency 2ω may be determined from the circuit equation,

$$V_2(G_2 + jB_2) + I_2 = 0 \quad (4.20)$$

in a self-consistent scheme. It may be found useful to get the first order solution from a 3-port model and use the solution to start the iteration in the 5-port model until self-consistency is reached. In the analysis of SIS quasiparticle mixer reported in Ref. [6] where the 3-port model serves to be a good approximation to the experimental situation, fast convergence in iteration in the 5-port model is achieved by this method. Self-consistency is reached with less than a hundred iterations.

V. PHOTON ASSISTED QUASIPARTICLE AND PAIR TUNNELING IN SIS MIXERS

The present quantum theory of SIS mixers proposed by Tucker only includes contributions from quasiparticle tunneling current. In order to get a complete picture of the performance of SIS mixers at high frequencies, it is necessary to include the effects of the pair tunneling

current in the theory of SIS mixers. The approach used by Tucker in his work on photon-assisted tunneling theory for quasiparticle mixing is here extended to include the effects of pair tunneling in SIS junctions. The admittance matrix elements are computed including both the quasiparticle and pair contributions. Once these admittance matrix elements are computed, the conversion loss and mixer noise temperature can be evaluated as before. The mathematical computation involved is tedious but straightforward and only the results are presented here.

We start with the transfer Hamiltonian

$$H_T = \sum_{kq} T_{kq} C_k^+ C_q + \sum_{kq} T_{kq}^* C_q^+ C_k . \quad (5.1)$$

proposed by Cohen, Falicov and Phillips [38]. T_{kq} represents the tunneling matrix element connecting state k on the left-hand side of the insulator with state q on the right-hand side, and C_k and C_q are one-electron operators on the left- and right-hand sides of the junction. The normal electron operators are related to the quasiparticle operators by the Bogoliubov transformation,

$$\gamma_{q\downarrow}^+ = u_q C_{q\downarrow}^+ - v_q C_{-q\downarrow} , \quad (5.2)$$

$$\gamma_{-q\downarrow} = u_q C_{-q\downarrow} + v_q C_{q\downarrow}^+ . \quad (5.3)$$

Following the approach used by Tucker, the total tunneling current density $I(t)$ as a function of time under external bias,

$$V(t) = V_0 + V_{LO}(t) , \quad (5.4)$$

can be calculated. Introducing the Fourier transform,

$$\exp \left[-\frac{ie}{\hbar} \int^t dt' V_{LO}(t') \right] = \int_{-\infty}^{\infty} d\omega W(\omega) e^{-i\omega t} , \quad (5.5)$$

the time dependent tunneling current is

$$I(t) = \text{Im} \left\{ \int_{-\infty}^{\infty} d\omega d\omega' W(\omega) W^*(\omega') e^{-i(\omega-\omega')} j_1(\omega + \frac{eV_0}{\hbar}) \right. \\ \left. + \int_{-\infty}^{\infty} d\omega d\omega' W(\omega) W(\omega') e^{-i(\omega+\omega'+\frac{2eV_0}{\hbar})t+i\theta} x j_2(\omega + \frac{eV_0}{\hbar}) \right\} \quad (5.6)$$

Equation (5.6) was first obtained by Werthamer [34]. The quantities j_1 and j_2 are complex quasiparticle and pair response functions as defined in the work by Werthamer [34] and Harris [35]. The first term in Eq. (5.6) represents quasiparticle contributions and is used by Tucker in his analysis of quasiparticle mixing. The second term in Eq. (5.6) represents pair contributions. From the small signal response, we can identify the admittance matrix element

$$Y_{mm'} = Y_{mm'qp} + Y_{mm'pair}, \quad (5.7)$$

which has been separated into terms involving quasiparticle contributions and pair contributions. The quasiparticle contribution is

$$\text{Re}(Y_{mm'qp}) = \text{Im} \int_{-\infty}^{\infty} d\omega \int_{-\infty}^{\infty} d\omega' W_{L0}(\omega) W_{L0}^*(\omega') \\ \times \frac{e}{2\hbar\omega_{m'}} \left\{ \delta(\omega-\omega'-\omega_m + \omega_{m'}) \left[j_1(\omega + \omega_{m'} + \frac{eV_0}{\hbar}) \right. \right. \\ \left. \left. - j_1(\omega + \frac{eV_0}{\hbar}) \right] \right. \\ \left. + \delta(\omega-\omega' + \omega_m - \omega_{m'}) \left[j_1(\omega + \frac{eV_0}{\hbar}) \right. \right. \\ \left. \left. - j_1(\omega - \omega_{m'} + \frac{eV_0}{\hbar}) \right] \right\}, \quad (5.8)$$

$$\begin{aligned}
 \text{Im}(Y_{mm'qp}) = & \text{Re} \int_{-\infty}^{\infty} d\omega \int_{-\infty}^{\infty} d\omega' W_{LO}(\omega) W_{LO}^*(\omega') \\
 & \times \frac{e}{2\hbar\omega_{m'}} \left\{ \delta(\omega - \omega' - \omega_m + \omega_{m'}) \left[j_l(\omega + \omega_m + \frac{eV_0}{\hbar}) \right. \right. \\
 & \quad \left. \left. - j_l(\omega + \frac{eV_0}{\hbar}) \right] \right. \\
 & - \delta(\omega + \omega' + \omega_m - \omega_{m'}) \left[j_l(\omega + \frac{eV_0}{\hbar}) \right. \\
 & \quad \left. \left. - j_l(\omega - \omega_{m'} + \frac{eV_0}{\hbar}) \right] \right\} \quad (5.9)
 \end{aligned}$$

The pair contribution is

$$\begin{aligned}
 \text{Re}(Y_{mm',\text{pair}}) = & \text{Im} \int_{-\infty}^{\infty} d\omega \int_{-\infty}^{\infty} d\omega' W_{LO}(\omega) W_{LO}^*(\omega') \\
 & \times \frac{e}{2\hbar\omega_{m'}} \left\{ \delta(\omega + \omega' - \omega_m + \omega_{m'} + \frac{2eV_0}{\hbar}) \left[e^{i\theta} j_2(\omega + \omega_{m'} + \frac{eV_0}{\hbar}) \right. \right. \\
 & \quad \left. \left. + e^{i\theta} j_2(\omega + \frac{eV_0}{\hbar}) \right] \right. \\
 & - \delta(\omega + \omega' + \omega_m - \omega_{m'} + \frac{2eV_0}{\hbar}) \left[e^{i\theta} j_2(\omega + \frac{eV_0}{\hbar}) \right. \\
 & \quad \left. \left. + e^{i\theta} j_2(\omega - \omega_{m'} + \frac{eV_0}{\hbar}) \right] \right\} \quad (5.10)
 \end{aligned}$$

$$\begin{aligned}
 \text{Im}(Y_{mm',\text{pair}}) = & \text{Re} \int_{-\infty}^{\infty} d\omega \int_{-\infty}^{\infty} d\omega' W_{L0}(\omega) W_{L0}(\omega') \\
 & \times \frac{e}{2\hbar\omega_{m'}} \left\{ \delta(\omega + \omega' - \omega_m + \omega_{m'} + \frac{2eV_0}{\hbar}) \left[e^{i\theta} j_2(\omega + \omega_{m'} + \frac{eV_0}{\hbar}) \right. \right. \\
 & \quad \left. \left. + e^{i\theta} j_2(\omega + \frac{eV_0}{\hbar}) \right] \right. \\
 & \delta(\omega + \omega' + \omega_m - \omega_{m'} + \frac{2eV_0}{\hbar}) \left[e^{i\theta} j_2(\omega + \frac{eV_0}{\hbar}) \right. \\
 & \quad \left. \left. + e^{i\theta} j_2(\omega - \omega_{m'} + \frac{eV_0}{\hbar}) \right] \right\} \quad (5.11)
 \end{aligned}$$

Once the admittance matrix elements are computed the mixer conversion loss can be calculated as in Eq. (2.11). The minimum detectable power can be evaluated as in reference [4]. Following Tucker's notation the noise current arising from shot noise under local oscillator drive within a bandwidth B can be calculated to be

$$[I_0]_{L0}^2 = B \sum_{m,m'} \lambda_{0m} \lambda_{0m'}^* H_{mm'} , \quad (5.12)$$

where

$$\lambda_{0m} = Z_{0m}/Z_{00} , \quad (5.13)$$

and the current correlation matrix is

$$\begin{aligned}
 H_{mm'} &= e \int \int d\omega d\omega' W(\omega) W^*(\omega') \delta(\omega' - \omega + \omega_{m'} - \omega_m) \\
 &\times \left\{ \coth \left[\frac{\beta}{2} (eV_0 + \hbar\omega' + \hbar\omega_m) \right] I_{qp} \left(V_0 + \frac{\hbar\omega'}{e} + \frac{\hbar\omega_{m'}}{e} \right) \right. \\
 &+ \coth \left[\frac{\beta}{2} (eV_0 + \hbar\omega - \hbar\omega_m) \right] I_{qp} \left(V_0 + \frac{\hbar\omega}{e} - \frac{\hbar\omega_{m'}}{e} \right) \Big\} \\
 &+ e \int \int d\omega d\omega' W(\omega) W^*(\omega') \delta \left(\omega' + \omega + \omega_{m'} - \omega_m + \frac{2eV_0}{\hbar} \right) \\
 &\times \coth \left[\frac{\beta}{2} (eV_0 + \hbar\omega' + \hbar\omega_m) \right] I_{pair} \left(V_0 + \frac{\hbar\omega'}{e} + \frac{\hbar\omega_{m'}}{e} \right) \\
 &+ e \int \int d\omega d\omega' W(\omega) W^*(\omega') \delta \left(\omega' + \omega - \omega_{m'} + \omega_m + \frac{2eV_0}{\hbar} \right) \\
 &\times \coth \left[\frac{\beta}{2} (eV_0 + \hbar\omega' - \hbar\omega_m) \right] I_{pair} \left(V_0 + \frac{\hbar\omega'}{e} - \frac{\hbar\omega_{m'}}{e} \right) \quad (5.14)
 \end{aligned}$$

Here $\beta = e/kT$ and $I_{qp}(V) = \text{Im} j_1(eV/\hbar)$ and $I_{pair}(V) = \text{Im} e^{i\theta} j_2(eV/\hbar)$ denote the quasiparticle and pair contributions to the dc I-V curve. The minimum detectable power is then given by Eq. (7.17) in reference [4] as

$$P_{det} = \frac{1}{4G_S |\lambda_{01}|^2} [I_0]_{L0}^2. \quad (5.15)$$

Although the quantum mixing theory presented here gives a complete description of the performance of SIS mixer its application is unfortunately not a trivial matter. This is due to several factors. The major problem is to determine the impressed local oscillator waveform $V_{LO}(t)$ and hence $W_{LO}(\omega)$. As the Josephson current is very sensitive to the ac admittance seen by the junction [39], the local oscillator waveform depends critically on the embedding admittance which appears across the junction. This includes admittances which exist in the external circuitry as well as the admittances corresponding to the resonance mode developed internally

inside the junction [40]. This situation is similar to the problems faced in Josephson devices [39,41]. In point-contact Josephson devices the problem is simplified by assuming the resistance-shunted-junction model. In the case of SIS mixers, a microscopic model is available but this adds complexity in solving the problem. The effects of pair tunneling on the dc I-V curves of SIS junctions have been treated by McDonald, Johnson and Harris [42]. In their work, the Fourier coefficient $W(\omega)$ is solved by iteration until self-consistency is reached. This method can be extended to calculate the conversion loss and noise of SIS mixers as once the Fourier coefficient $W(\omega)$ is obtained the admittance matrix element can be calculated from Eqs. (5.8) to (5.11). From $W(\omega)$, $V_{L0}(t)$ and $I(t)$ can be calculated from Eq. (5.5) and (5.6). When $V_{L0}(t)$ and $I(t)$ are expanded into their Fourier components I_ω and V_ω , these must satisfy the circuit equation

$$I_\omega + V_\omega \cdot Y_\omega = I_p, \quad (5.16)$$

$$I_{\omega'} + V_{\omega'} \cdot Y_{\omega'} = 0, \quad \omega' \neq \omega, \quad (5.17)$$

where I_p is the source current amplitude at the local oscillator frequency ω , and Y_ω is the embedding admittance at frequency ω . Since Eqs. (5.5), (5.6), (5.16) and (5.17) have to be satisfied at all frequencies and at all dc bias voltages, the problem has to be solved self-consistently.

The method discussed in Section IV may be used to determine the local oscillator waveform by treating the embedding admittances as variable parameters in fitting to the experimental dc I-V curves. Alternatively, with a knowledge of the admittances in the embedding network, conventional self-consistent methods [17,36] used in classical mixer analysis can be employed to determine the local oscillator waveform with classical expressions replaced by quantum expressions where appropriate.

VI. PERFORMANCE LIMIT OF SIS MIXERS

When an SIS junction is under constant dc current bias, a 'drop-back' voltage exists at which the dc I-V curve switches hysteretically to zero voltage [6,12,14,43]. This phenomena

can be understood by the fact that in practical situations the finite junction capacitance is not capable of shorting out the low frequency Josephson currents generated at low voltages. As a result, pair contributions to the dc I-V curve becomes more and more significant at low voltages. A negative resistance region will then develop on the dc I-V curve which will hysteretically switch to zero voltage when the junction is biased with a constant dc current source. For the same reason, in the operation of SIS quasiparticle mixers Josephson noise will become significant when the local oscillator voltage swing is so large that the instantaneous bias voltage is driven below the drop-back voltage. The junction capacitance is then no longer large enough to short out these low frequency Josephson currents. This explanation is consistent with the empirical results observed in the recent report on mixing using SIS arrays [14].

Extended negative-resistance region on the I-V curves of very small area SIS tunnel junctions has been observed by Buckner, Chen and Langenberg [44]. This type of I-V characteristics has been analyzed by using the resistance-shunted model with a capacitive load [39,45]. A more exact analysis of the effects of junction capacitance on the dc I-V curves of SIS tunnel junctions using weak-coupling superconductivity tunneling theory can be found in the work by McDonald, Johnson and Harris [42]. All these experimental and theoretical results indicate that an extended negative resistance region will develop on the I-V curves of small capacitance SIS tunnel junctions. Hence, under a constant dc current bias the junction will hysteretically switch to zero voltage. Another important empirical fact which has been observed [14,43] is that the drop-back voltage is found to be proportional to the Josephson plasma frequency voltage. In this section, the theoretical formalism presented in Section V is used to obtain an estimation of the value of the drop-back voltage. An approximate expression for the drop-back voltage is obtain which is proportional to the Josephson plasma frequency voltage as experimentally observed.

We consider an SIS junction under constant dc current bias and assume that at all ac frequencies the junction is terminated by its own capacitance. The voltage across the junction will consist of a dc component V_0 as well as Fourier components at the harmonics of the Josephson frequency

$$\omega_J = \frac{2eV_0}{\hbar} . \quad (6.1)$$

For voltages V_0 above the drop-back voltage the Josephson frequency will be high. An analytic first order solution can then be solved self-consistently. In this voltage region we may approximate the time dependent voltage across the junction to be

$$V(t) = V_0 + V_1 \cos \omega_J t , \quad (6.2)$$

and assume that all the high harmonics of the Josephson frequency are being shorted out by the junction capacitance. The condition for Eq. (6.2) to be valid is

$$\frac{V_1}{V_0} \leq \epsilon < 1 . \quad (6.3)$$

The value of ϵ will be determined later by comparing with experimental results. We shall determine the value of V_1 self-consistently through the circuit equation,

$$I_{qp}(t) + I_{pair}(t) + C \frac{dV(t)}{dt} = I_0 , \quad (6.4)$$

where $I_{qp}(t)$ denotes the quasiparticle current, $I_{pair}(t)$ denotes the pair current, C is the junction capacitance and I_0 is the external dc bias current. Condition (6.3) will then be used to give an estimation of the drop-back voltage.

From Eq. (5.6), we have

$$I_{qp}(t) = \text{Im} \sum_{n=-\infty}^{\infty} \sum_{m=-\infty}^{\infty} J_n(z) J_{n+m}(z) j_1((n+\frac{1}{2})\omega_J) \\ \times e^{im\omega_J t} . \quad (6.5)$$

$$I_{pair}(t) = \text{Im} \sum_{n=-\infty}^{\infty} \sum_{m=-\infty}^{\infty} J_n(z) J_{-n-m-1}(z) e^{i\theta} j_2((n+\frac{1}{2})\omega_J) \\ \times e^{im\omega_J t} , \quad (6.6)$$

where

$$z = \frac{eV_1}{\hbar\omega_J} . \quad (6.7)$$

From Eq. (6.3) we have

$$z = \frac{V_1}{2V_0} \ll 1 . \quad (6.8)$$

To the first order of z and for $V_0 < 2\Delta/e$, we may write Eqs. (6.5) and (6.6) as

$$\begin{aligned} I_{qp}(t) = & \frac{z}{2} \left[\operatorname{Re} j_1 \left(\frac{1}{2}\omega_J \right) - \operatorname{Re} j_1 \left(\frac{3}{2}\omega_J \right) \right] \sin \omega_J t \\ & + \frac{z}{2} \left[\operatorname{Im} j_1 \left(\frac{3}{2}\omega_J \right) \right] \cos \omega_J t , \end{aligned} \quad (6.9)$$

$$\begin{aligned} I_{pair}(t) = & -z \left[\operatorname{Re} j_2 \left(\frac{1}{2}\omega_J \right) \right] \sin \theta \\ & - \left[\operatorname{Re} j_2 \left(\frac{1}{2}\omega_J \right) \right] \cos \theta \cdot \sin \omega_J t \\ & + \left[\operatorname{Re} j_2 \left(\frac{1}{2}\omega_J \right) \right] \sin \theta \cdot \cos \omega_J t . \end{aligned} \quad (6.10)$$

We have used the fact that $\operatorname{Im} j_1 \left(\frac{1}{2}\omega_J \right) = 0$ and $\operatorname{Im} j_2 \left(\frac{1}{2}\omega_J \right) = 0$ for $V_0 < 2\Delta/e$. Note that

$\operatorname{Re} j_2(\omega)$ is negative [35].

Substituting Eqs. (6.9) and (6.10) into Eq. (6.4), we get the following equations for dc, $\sin \omega_J t$ and $\cos \omega_J t$ components:

$$-z \left[\operatorname{Re} j_2 \left(\frac{1}{2}\omega_J \right) \right] \sin \theta = I_0 , \quad (6.11)$$

$$\frac{z}{2} \left[\operatorname{Re} j_1 \left(\frac{1}{2} \omega_j \right) - \operatorname{Re} j_1 \left(\frac{3}{2} \omega_j \right) \right] - \operatorname{Re} j_2 \left(\frac{1}{2} \omega_j \right) \cos \theta$$

$$- \omega_j C V_1 = 0 . \quad (6.12)$$

$$\frac{z}{2} \operatorname{Im} j_1 \left(\frac{3}{2} \omega_j \right) + \operatorname{Re} j_2 \left(\frac{1}{2} \omega_j \right) \sin \theta = 0 . \quad (6.13)$$

We see from Eq. (6.13) that $\sin \theta \sim z$ and $\cos \theta \sim 1$. From Eq. (6.12) we have

$$V_1 \approx \left| \frac{\operatorname{Re} j_2 \left(\frac{1}{2} \omega_j \right)}{\omega_j C} \right|$$

$$= \left| \frac{\operatorname{Re} j_2 \left(\frac{1}{2} \omega_j \right)}{\frac{2eV_0}{\hbar} \cdot C} \right| . \quad (6.14)$$

Equation (6.14) gives

$$V_0 V_1 = \left| \frac{\hbar \cdot \operatorname{Re} j_2 \left(\frac{1}{2} \omega_j \right)}{2eC} \right|$$

$$= \left| \frac{\operatorname{Re} j_2 \left(\frac{1}{2} \omega_j \right)}{\operatorname{Re} j_2(0)} \right| \cdot \left| \frac{\hbar \operatorname{Re} j_2(0)}{2eC} \right|$$

$$= \left| \frac{\operatorname{Re} j_2 \left(\frac{1}{2} \omega_j \right)}{\operatorname{Re} j_2(0)} \right| \cdot V_{pl}^2 . \quad (6.15)$$

where

$$V_{pl} = \left| \frac{\hbar I_c}{2eC} \right|^{\frac{1}{2}} \quad (6.16)$$

is the plasma frequency voltage and $I_c = |\operatorname{Re} j_2(0)|$. The voltage limit governing the inequality in

(6.3) may be used to give an estimation of the value of the drop-back voltage V_d . Substituting $V_1/V_d = \epsilon$ at $V_0 = V_d$ in Eq. (6.15) we have

$$V_d = \epsilon^{-\frac{1}{4}} \left| \frac{\text{Rej}_2(\frac{1}{2}\omega_1)}{\text{Rej}_2(0)} \right|^{\frac{1}{2}} \cdot V_{pl} . \quad (6.17)$$

At temperatures well below T_c , it was found experimentally that $V_d/V_{pl} \approx \epsilon^{-\frac{1}{4}} \approx 3$ [14]. A value of $V_d/V_{pl} \approx 3.5$ can be attributed to the junction ($2\Delta R_N C/\hbar \approx 40$) used in reference [6]. Based on this empirical fact, a value of $\epsilon \approx 0.1$ will be used in Eq. (6.17) to obtain a general expression for the drop-back voltage. The solution of the drop-back voltage V_d as a function of plasma frequency voltage V_{pl} and $R_N C$ time constant is shown in Fig. 8. For $V_0 > V_d$, from Eq. (6.11), I_0 increases roughly as $z^2 \sim 1/V_0^4$ as V_0 is decreased. This gentle negative resistance region may often be masked by leakage currents in real junctions. For $V_0 < V_d$, Josephson contribution becomes more and more significant and the negative resistance region becomes more pronounced. Under constant current bias an SIS junction will hysteretically switch to zero voltage at a voltage equal to the drop-back voltage V_d . For some voltage region near the gap voltage $2\Delta/e$, conditions (6.3) and (6.15) will not be satisfied because of the presence of the Riedel singularity at $\text{Rej}_2(2\Delta/\hbar)$. In this voltage region the I-V curve will be rounded by the pair contribution.

Equation (6.17) may be used to give an upper frequency limit at which SIS mixers can be operated without the strong influence of the Josephson effects. As the instantaneous bias point of SIS mixers should not be driven by the local oscillator below V_d , the upper frequency limit can be defined as the frequency ω at which the first photon peak falls midway between the drop-back voltage and the gap voltage. The junction can then be operated at the first photon peak and with the instantaneous bias point being driven by the local oscillator into the non-linear region of the I-V curve without suffering from the Josephson noise. As the first photon peak appears at half of $\hbar\omega/e$ from the gap voltage we have

$$\hbar\omega = 2\Delta - eV_d . \quad (6.18)$$

Solutions of Eq. (6.18) are shown in Fig. 9. The upper frequency limit will depend on the $R_N C$ time constant of the junction, where R_N is the normal resistance of the junction at high voltages. For a junction with an infinitely large capacitance the drop-back voltage is zero and Eq. (6.18) gives an upper frequency limit of $2\Delta/h$. For a given $R_N C$ time constant Fig. 9 can be used to give the highest operational frequency of the junction. A more practical way to look at Eq. (6.18) is that it gives the highest operational frequency and the corresponding $R_N C$ time constant of the junction for a given $\omega C R_N$ product for effective RF coupling. For $\omega C R_N = 1$, Eq. (6.18) gives $\hbar\omega/2\Delta \sim 0.14$ which corresponds to an upper frequency limit of ~ 100 GHz for Pb junctions ($2\Delta/h \sim 800$ GHz). These theoretical predictions agree well with the empirical results reported in reference [14]. Higher operating frequencies are possible with a higher $\omega C R_N$ product. For $\omega C R_N = 5$, the upper frequency limit is increased to $\hbar\omega/2\Delta \sim 0.40$ corresponding to ~ 300 GHz for Pb.

In the operation of SIS quasiparticle mixers it appears to be beneficial to operate with a large $R_N C$ time constant ($\omega C R_N > 1$). This has two major advantages. A large $R_N C$ time constant will reduce harmonic conversion in SIS quasiparticle mixing near the gap voltage and improve the conversion efficiency of fundamental mixing [6,10,14]. At the same time, large $R_N C$ time constant will have a smaller drop-back voltage and hence a higher operational frequency. This condition of large $\omega C R_N$ product is contradictory to the apparent requirement that the $R_N C$ product has to be minimized for effective RF power coupling. This requirement is necessary in devices such as Schottky and super-Schottky diodes in which the presence of series resistance R_S has limited the operation frequency ω to less than approximately $1/C\sqrt{R_{in}R_S}$, where R_{in} is the input impedance of the junction at the RF frequency. This is due to the fact that the junction capacitance has to be charged and discharged through the series resistance each local oscillator cycle. At temperature well below T_c , series resistance is negligible in SIS junctions. The presence of junction capacitance would not then impose such a serious problem on effective RF power coupling. In principle the junction capacitance can always be resonated out by external microwave circuitry, although in reality circuit losses impose practical limits to the degree to which this can be achieved. In the quasiparticle mixing experiment at 36 GHz in which

conversion gain is reported [6], an operating condition of $\omega CR_N \approx 2$ is used. Computer simulations on the mixing experiments have indicated that the junction capacitance is effectively resonated out by the matching network. The tradeoff in using junctions with large ωCR_N product is that it leads to a small bandwidth and to practical difficulties in realizing the tuning and matching circuits. In this respect it seems that the upper frequency limit of SIS quasiparticle mixers is governed by the practical limit of the largest ωCR_N product acceptable for effective RF power coupling.

In order to examine the significance of the harmonic contents of the Josephson frequency, a similar analysis has been performed by including the harmonic content $V_2 \cos 2\omega_J t + V'_2 \sin 2\omega_J t$ in Eq. (6.2) and a set of equations similar to Eqs. (6.11) to (6.13) is obtained. For each pair of values of $R_N C$ and the corresponding V_d given by Eq. (6.17) (see Fig. 8), the values of V_2 and V'_2 are calculated. It is found that in all cases $|V_2/V_1| < 0.025$ and $|V'_2/V_1| < 0.017$. Hence it is well justified in ignoring the harmonic contents of the Josephson frequency in Eq. (6.2). In Eq. (6.17) the value of $\epsilon = 0.1$ is used in arriving at the solutions presented in Figs. 8 and 9. This value is obtained by comparing Eq. (6.17) with the experimental results that $V_d/V_m \approx 3$ to 3.5 for junctions with $2\Delta R_N C/\hbar \approx 40$. Whether the same value of ϵ should be used throughout the entire range of $R_N C$ remains a question. At values of $2\Delta R_N C/\hbar \leq 10$ the observed drop-back voltage seems to be much lower than that predicted by this model [37].

VII. CONCLUSION

Due to the strong nonlinearity on the I-V curve of SIS junctions, SIS quasiparticle mixers can be operated in the quantum limit in which the classical prohibition of conversion gain in resistive mixing is removed. Under proper bias conditions, stable mixing with conversion gain is possible. By using the 3-pot Y-mixer model it is demonstrated that the S-shape tunneling structure at the gap voltage of the I-V curve of SIS junctions is essential in achieving conversion gain. The role played by the nonlinear quantum susceptance in frequency conversion is discussed. It is found that the nonlinear quantum susceptance is not essential for achieving

conversion gain. In analyzing a mixing experiment the determination of the impressed local oscillator waveform and the embedding admittance has remained a difficult problem. A new method is introduced in the analysis of SIS mixing experiments. The impressed local oscillator waveform and the embedding admittance are deduced from the dc I-V curve measured at various local oscillator power levels. In order to take into account the effects of pair tunneling in SIS mixers, the photon-assisted quasiparticle tunneling theory proposed by Tucker is extended to include the pair tunneling contribution. The admittance matrix element, which includes both the quasiparticle and pair contributions, is calculated. This is essential to give a complete picture of the performance of SIS mixers. An explanation of the experimentally observed drop-back voltage is suggested. An expression for the drop-back voltage is obtained by using the complete quasiparticle and pair tunneling theory. The upper frequency limit at which SIS quasiparticle mixers can operate without the strong influence of the Josephson noise is calculated. This upper frequency limit depends on the largest ωCR_N product acceptable for effective RF coupling. If a sufficiently effective RF matching network can be designed it is very likely that low noise and stable mixing with conversion gain can be achieved by SIS quasiparticle mixers over the whole millimeterwave band to ~ 300 GHz. An absolute upper frequency limit for SIS quasiparticle mixers would be the superconducting gap frequency at which superconducting pair breaking begins.

VIII. Acknowledgement

The author wishes to thank Professor P. L. Richards, M. J. Feldman, A. R. Kerr, S. Weinreb, L. R. D'Addario, and J. R. Tucker for many critical comments in connection with this work. A portion of this research was supported by the U. S. Office of Naval Research. The author is grateful to Bell Laboratories for the help provided towards the completion of this paper.

REFERENCES

- [1] F. L. Vernon, Jr., M. F. Millea, M. F. Bottjer, A. H. Silver, R. J. Pederson, and M. McColl, "The super-Schottky diode," *IEEE Trans. Microwave Theory Tech.*, vol. MTT-25, pp. 286-294, April 1977.
- [2] M. McColl, M. F. Millea, A. H. Silver, M. F. Bottjer, R. J. Pederson and F. L. Vernon, Jr., "The super-Schottky microwave mixer," *IEEE Trans. Magn.*, vol. MAG-13, pp. 221-227, January 1977.
- [3] M. McColl, M. F. Bottjer, A. B. Chase, R. J. Pederson, A. H. Silver, and J. R. Tucker, "The super-Schottky diode at 30 GHz," *IEEE Trans. Magn.*, vol. MAG-15, pp. 468-470, January 1979.
- [4] J. R. Tucker, "Quantum limited detection in tunnel junction mixers," *IEEE J. Quantum Elect.*, vol. QE-15, pp. 1234-1258, November 1979.
- [5] P. L. Richards, T. M. Shen, R. E. Harris, and F. L. Lloyd, "Quasiparticle heterodyne mixing in SIS tunnel junctions," *Appl. Phys. Lett.*, vol. 34, pp. 345-347, May, 1979.
- [6] T. M. Shen, P. L. Richards, R. E. Harris and F. L. Lloyd, "Conversion gain in mm-wave quasiparticle heterodyne mixers," *Appl. Phys. Lett.*, vol. 36, pp. 777-779, May, 1980.
- [7] G. J. Dolan, T. G. Phillips, and D. P. Woody, "Low noise 115 GHz mixing in superconducting oxide barrier tunnel junctions," *Appl. Phys. Lett.*, vol. 34, pp. 347-349, March 1979.
- [8] S. Rudner and T. Claeson, "Analysis of superconducting tunnel junctions as low-noise 10 GHz mixers," *Appl. Phys. Lett.*, vol. 34, pp. 711-713, May, 1979.
- [9] J. R. Tucker, "Predicted conversion gain in superconductor-insulator-superconductor quasiparticle mixers," *Appl. Phys. Lett.*, vol. 36, pp. 477-479, March 1980.
- [10] P. L. Richards and T. M. Shen, "Superconductive devices for millimeter wave detection

mixing and amplification," *IEEE Trans. on Electron Devices*, vol. ED-27, pp. 1909-1920, Oct., 1980.

- [11] T. M. Shen, P. L. Richards, R. E. Harris and F. L. Lloyd, "SIS quasiparticle junctions as microwave photon detectors and mixers with conversion gain," *APS meeting*, New York, N. Y., March 24-28, 1980.
- [12] G. J. Dolan, R. A. Linke, T. C. L. G. Sollner, D. P. Woody, and T. G. Phillips, "Superconducting tunnel junctions as mixers at 115 GHz," *IEEE Trans. Microwave Theory and Techniques*, vol. MTT-29, pp. 87-91, Feb., 1981.
- [13] T. M. Shen and P. L. Richards, "Computer simulations of the performance of quasiparticle heterodyne mixers," *IEEE Trans. Magn.*, vol. MAG-17, pp. 677-683, Jan. 1981.
ERRATA: p. 680, when finite leakage current is included in the SIS quasiparticle mixer analysis, the contour $L = 0$ falls as $P_{L0}^{\frac{1}{2}}$, not as $P_{L0}^{1/3}$.
- [14] S. Rudner, M. J. Feldman, E. Kollberg and T. Claeson, "The antenna - coupled SIS quasiparticle array mixer," *IEEE Trans. Magn.*, vol. MAG-17, pp. 690-693, Jan. 1981.
- [15] H. C. Torrey and C. A. Whitmer, *Crystal Rectifiers*, M.I.T. Rad. Lab. Series, vol. 15, McGraw Hill, 1948.
- [16] A. A. M. Saleh, *Theory of Resistive Mixers*, M.I.T. Press, Cambridge, Massachusetts, 1971.
- [17] D. N. Held and A. R. Kerr, "Conversion loss and noise of microwave and millimeter-wave mixers: Part 1-Theory," *IEEE Trans. Microwave Theory Tech.*, vol. MTT-26, pp. 49-55, Feb. 1978.
- [18] J. M. Manley and H. E. Rowe, "Some general properties of nonlinear elements," *Proc. IRE*, vol. 44, pp. 904-913, July, 1956.
- [19] C. Dragone, "Analysis of thermal and shot noise in pumped resistive diodes," *Bell System Tech. J.*, vol. 47, pp. 1883-1902, November 1968.

- [20] A. Uhlir, Jr., "Shot noise in p-n junction frequency converters," *Bell System Tech. J.*, vol. 37, pp. 951-988, July 1958.
- [21] E. W. Herold, R. R. Bush and W. R. Ferris, "Conversion loss of diode mixers having image-frequency impedance," *Proc. I.R.E.* vol. 33, pp. 603-609, September 1945.
- [22] C. H. Page, "Frequency conversion with positive nonlinear resistors," *J. of Research of N.B.S.*, vol. 56., pp. 179-182, April 1956.
- [23] R. H. Pantell, "General power relationships for positive and negative resistive elements," *Proc. I.R.E.*, vol. 46, pp. 1910-1913, December 1958.
- [24] G. C. Messenger, "Theory and operation of crystal diodes as mixers," *Proc. I.R.E.* vol. 45, pp. 1269-1283, September 1957.
- [25] S. Egami, "Nonlinear, linear analysis and computer-aided design of resistive mixers," *IEEE, Trans. Microwave Theory Tech.*, vol. MTT-22, pp. 270-275, March 1973.
- [26] L. Mania and G. B. Stracca, "Effects of the diode junction capacitance on the conversion loss of microwave mixers," *IEEE, Trans. on Communications*, vol. COM-22, pp. 1428-1435, September 1974.
- [27] M. R. Barber, "Noise figure and conversion loss of the Schottky barrier mixer diode," *IEEE, Trans. Microwave Theory Tech.*, vol. MTT-15, pp. 629-635, November 1967.
- [28] R. L. Eisenhart and P. J. Khan, "Theoretical and experimental analysis of a waveguide mounting structure," *IEEE Trans. Microwave Theory Tech.*, vol. MTT-19, pp. 706-719, Aug., 1971.
- [29] D. N. Held and A. R. Kerr, "Conversion loss and noise of microwave and millimeter-wave mixers: Part II - experiments," *IEEE Trans. Microwave Theory Tech.*, vol. MTT-26, pp. 55-61, Feb., 1978.
- [30] C. E. Hagström and E. L. Kollberg, "Measurements of embedding impedance of millimeterwave diode mounts," *IEEE, Trans. Microwave Theory Tech.*, vol. MTT-28, pp. 899-904, Aug. 1980.

- [31] A. R. Kerr, private communication.
- [32] P. Penfield and R. Rafuse, *Varactor Applications*, M.I.T. Press, 1962.
- [33] C. S. Kim, "Tunnel-diode converter analysis," *I.R.E., Trans. Electron Devices*, vol. ED-8, pp. 394-405, September 1961.
- [34] N. R. Werthamer, "Nonlinear self-coupling of Josephson radiation in superconducting tunnel junctions," *Phys. Rev.*, vol. 147, pp. 255-263, July, 1966.
- [35] R. E. Harris, "Cosine and other terms in the Josephson tunneling current," *Phys. Rev. B*, vol. B 10, pp. 84-94, July 1974.
- [36] A. R. Kerr, "A technique for determining the local oscillator waveforms in a microwave mixer," *IEEE Trans. Microwave Theory Tech.*, vol. MTT-23, pp. 828-931, Oct. 1975.
- [37] M. J. Feldman, private communication.
- [38] M. H. Cohen, L. M. Falicov, and J. C. Phillips, "Superconductive tunneling," *Phys. Rev. lett.*, vol. 8, pp. 316-318, April 1962.
- [39] D. E. McCumber, "Effect of ac impedance on dc voltage - current characteristics of superconductor weak-link junctions," *J. of Appl. Phys.*, vol. 39, pp. 3113-3118, June, 1968.
- [40] D. D. Coon and M. D. Fiske, "Josephson ac and step structure in the supercurrent tunneling characteristic," *Phys. Rev.*, vol. 138, pp. A744-A746, May 1965.
- [41] Y. Taur, "Josephson junction mixer analysis using frequency-conversion and noise correlation matrices," *IEEE Trans. on Electron Devices*, vol. ED-27, pp. 1921-1928, Oct., 1980.
- [42] D. G. McDonald, G. G. Johnson, and R. E. Harris, "Modeling Josephson junctions," *Phys. Rev.*, vol. B 13, pp. 1028-1031, February, 1976.
- [43] N. F. Pedersen, J. Mygind, O. H. Soerensen and B. Dueholm, "A simple qualitative determination of Josephson tunnel junction parameters near the transition temperature," *J. de Physique*, vol. 39, pp. C6-1232-1233, August 1978.

- [44] S. A. Buckner, J. T. Chen and D. N. Langenberg, "Current characteristics of small Josephson tunnel junctions," *Phys. Rev. Lett.*, vol. 25, pp. 738-741, September 1970.
- [45] Yu. M. Ivanchenko and L. A. Zil'berman, Sov. *Phys. JETP*, vol. 28, pp. 1272-1276, June 1969.

Table 1: 3-port Y-mixer calculation of the conversion efficiency expected for the SIS mixing experiment reported in reference [6]. Double sideband (DSB) conversion efficiencies are calculated at the first four photon peaks from the gap voltage. Conversion efficiencies L^{-1} in column one are calculated by using the full quantum admittance matrix elements. Conversion efficiencies L'^{-1} in column two are calculated by using only the quantum conductive terms. Contributions from the non-linear quantum susceptive terms are examined by taken the ratio L^{-1}/L'^{-1} which is shown in column three. Experimentally conversion gain was observed at the fourth photon peak.

Bias point	L^{-1}	L'^{-1}	L^{-1}/L'^{-1}
1st photon peak	5.40	1.69	3.20
2nd photon peak	2.30	1.75	1.31
3rd photon peak	1.64	1.53	1.07
4th photon peak	1.33	1.31	1.02

FIGURE CAPTIONS

- Fig. 1 Y-mixer equivalent circuit.
- Fig. 2 Quasiparticle response function of ideal SIS junction with identical superconductors at $T=0$. The I-V curve of the junction is given by the imaginary part of the response function. The "photon points" on the I-V curve are represented by A and B.
- Fig. 3 Quasiparticle response function of ideal SIN junction at $T=0$.
- Fig. 4 SSB conversion loss L^0 (in unit of G_{10}/G_{01}) of resistive mixers as a function of source conductance G_S (in unit of G_{11}) with η as parameter as calculated from the 3-port Y-mixer model. The situation for $\eta < 1$ is illustrated by the case $\eta = 0.9$ and the situation for $\eta > 1$ is illustrated by $\eta = 1.1$. For $\eta < 1$, minimum conversion loss occurs at the source conductance of $G_S/G_{11} = \sqrt{1-\eta}$. As η approaches to 1, the minimum conversion loss approaches to the value of $2G_{10}/G_{01}$ with optimal source conductance G_S/G_{11} approaches to zero. Gain (SSB $L^0 < 2$) is possible for $G_{10}/G_{01} < 1$. For $\eta > 1$, negative IF conductance (corresponds to $L^0 < 0$) occurs for $G_S/G_{11} < \eta - 1$. Stable mixing with gain is possible for values of $G_S/G_{11} \geq \eta - 1$. (0.1 to 0.45 in our example of $\eta = 1.1$).
- Fig. 5 Network analysis of SIS mixer showing equivalent circuit at the local oscillator frequency. The junction is represented by the nonlinear resistive element. Junction capacitance is considered as part of the source admittance.
- Fig. 6 Graphical method in determining the source admittance of the embedding network. In this (G_S, B_S) phase diagram, different circles C_1, C_2 and C_3 correspond to different values of V_0 and/or P_{LO} . Within the validity of the 3-port model, all the circles should intersect at one point which is the source admittance.

- Fig. 7 Experimental I-V curve of a typical SIS junction used in mixing experiments (a) without and (b) with local oscillator power. Dotted curve (c) is a theoretical curve calculated with a source admittance of $0.07 - j0.007 \Omega^{-1}$ determined by the method discussed using a 3-port model.
- Fig. 8 Drop-back voltage V_d as a function of plasma frequency voltage V_p and $R_N C$ time constant. The set of solutions of V_d which occurs beyond the maximum (minimum) of $V_p(R_N C)$ corresponds to the rounding of the corner of the I-V curve near the gap voltage $2\Delta/e$.
- Fig. 9 Upper frequency limit of SIS quasiparticle mixing governed by the onset of the Josephson effects at the first and second photon peaks (measured from the gap voltage $2\Delta/e$) with a local oscillator drive which just reaches into the nonlinear region of the I-V curve at the gap voltage. The dash lines represent the positions of the lowest voltage reached by the instantaneous bias point which should remain above the drop-back voltage. For a given acceptable operating condition of ωCR_N product the maximum operating frequency is given by the intersecting point at which the dash line of the first photon peak crosses the ωCR_N contour. These curves can also be used to find the maximum operation frequency possible for a given junction ($R_N C$ time constant), or the minimum $R_N C$ time constant required for a given operation frequency.

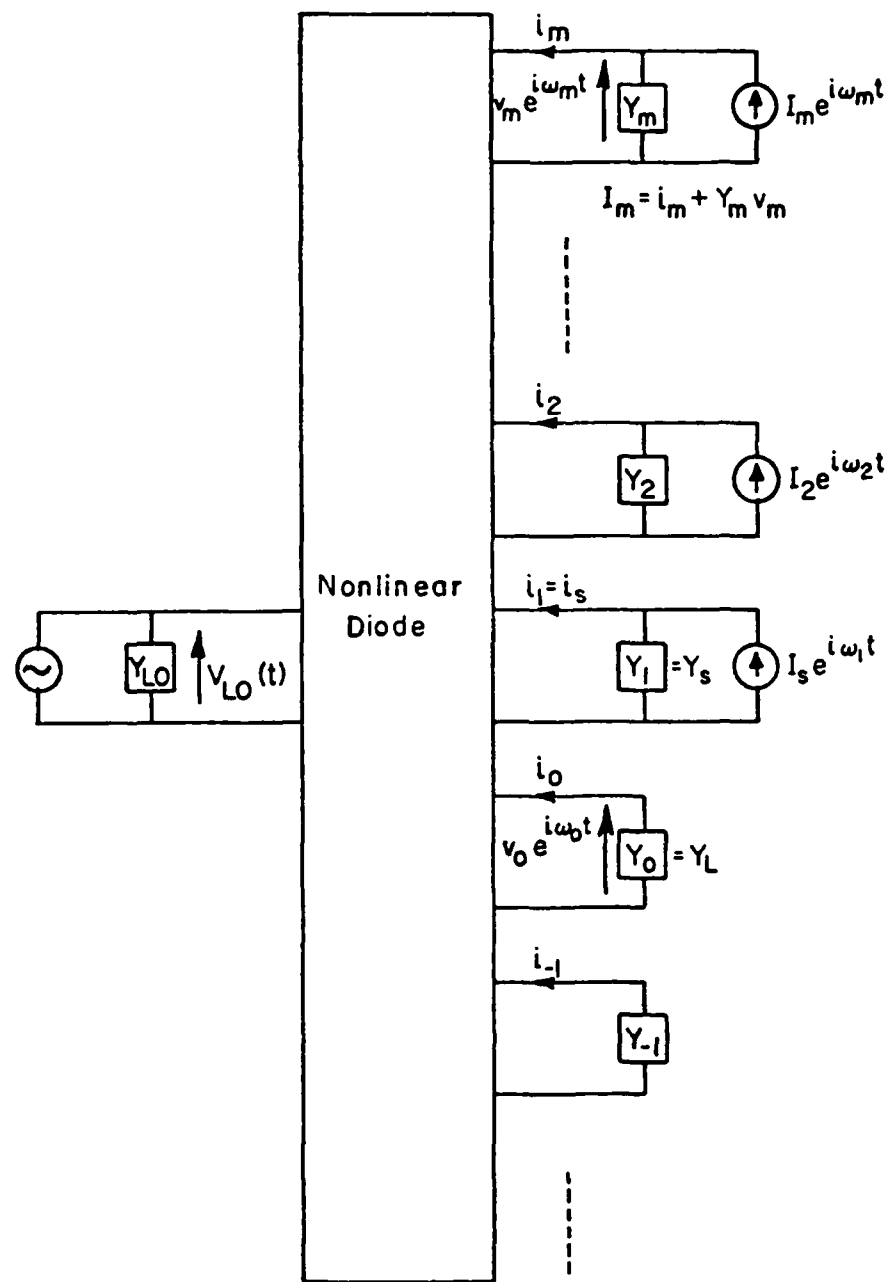


Fig. 1

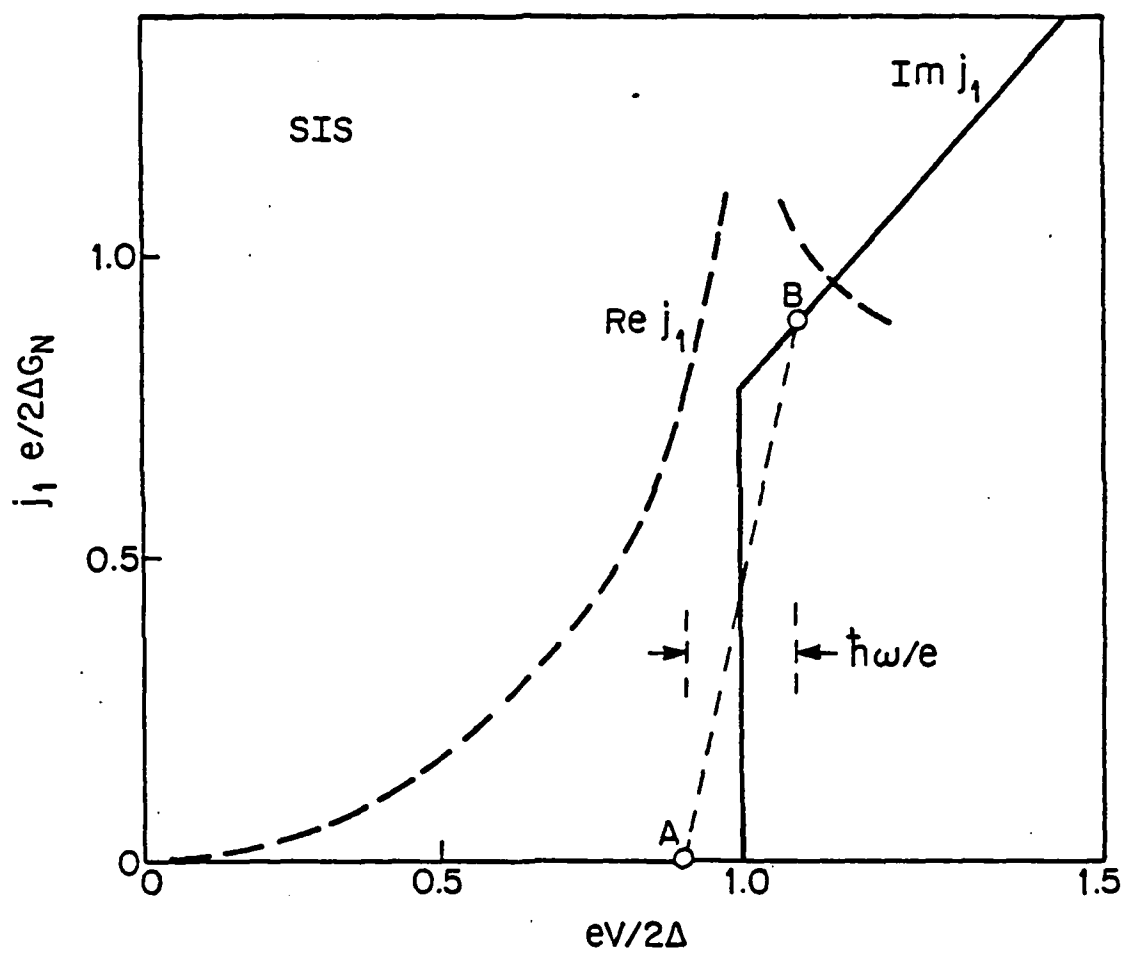


Fig. 2
 cor/CH/327

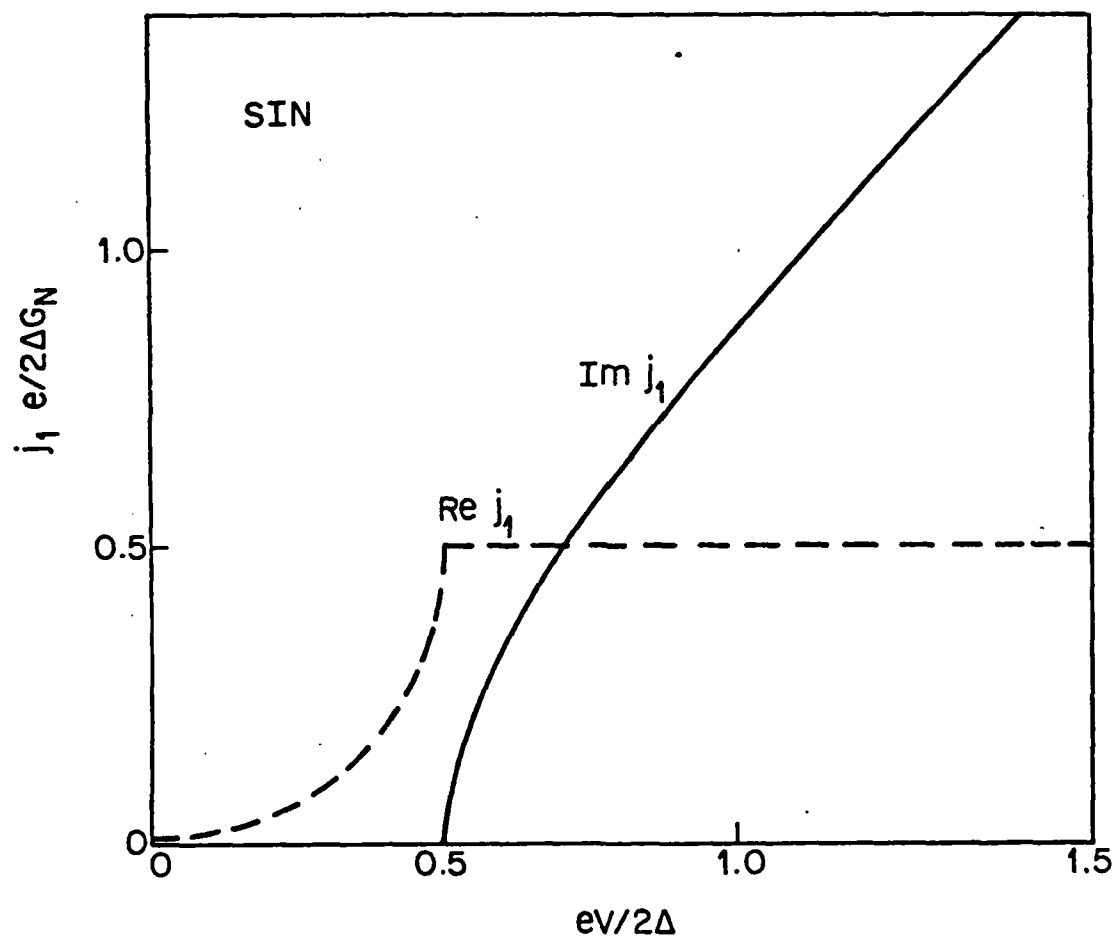


Fig. 3

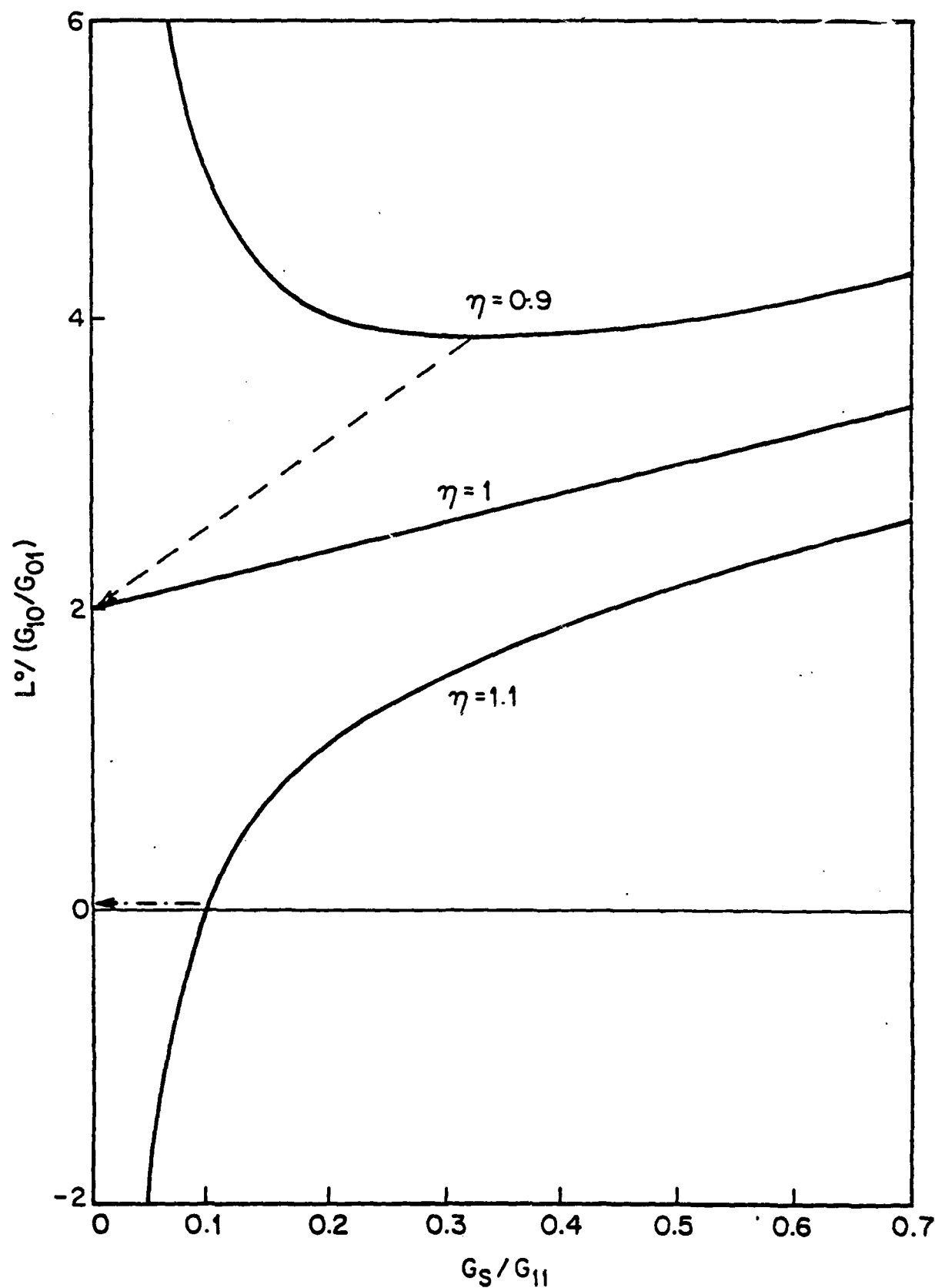


Fig. 4

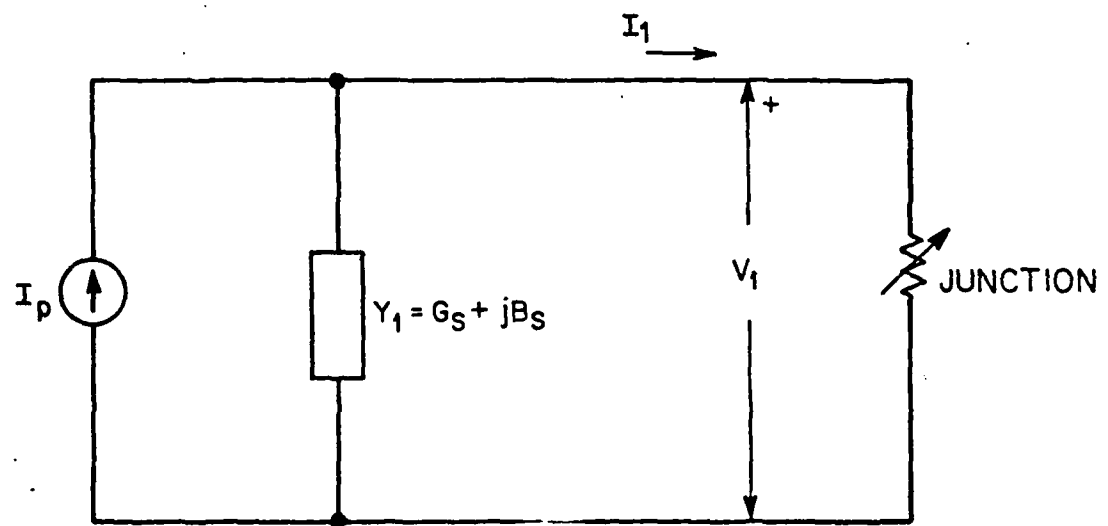


Fig. 5

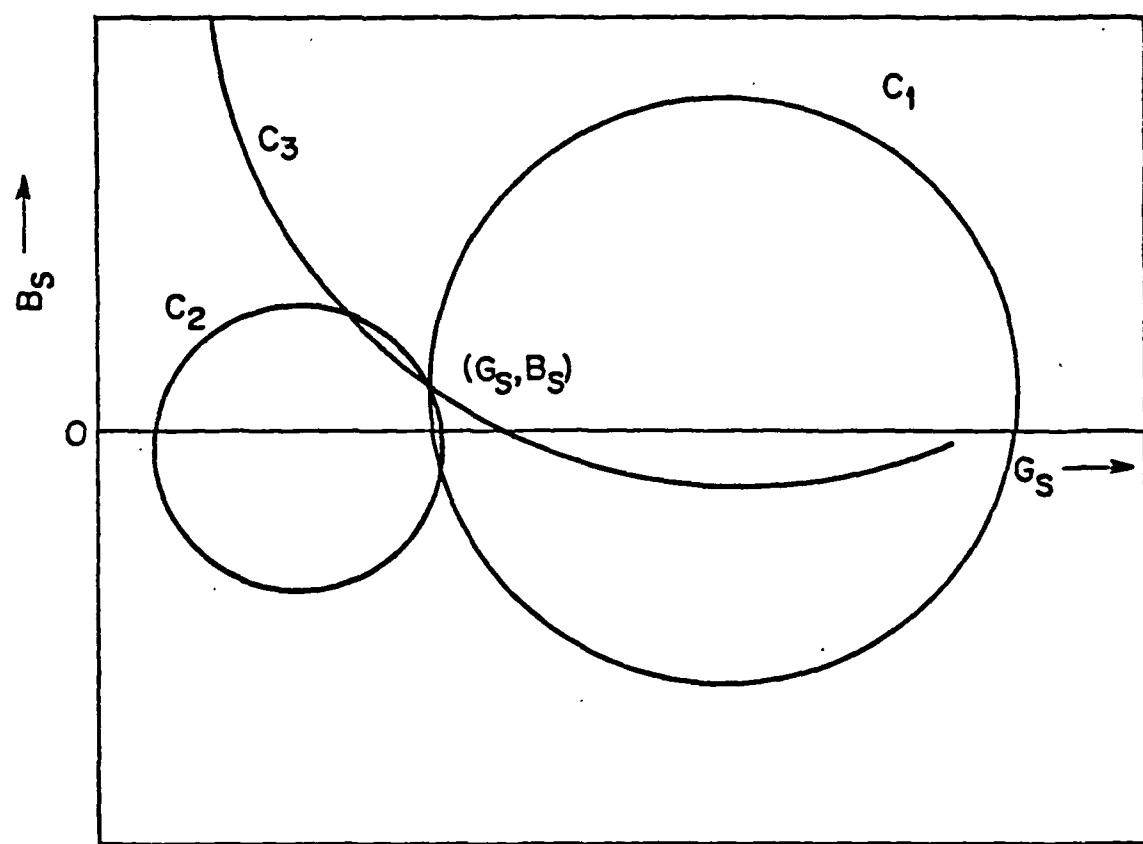


Fig. 6

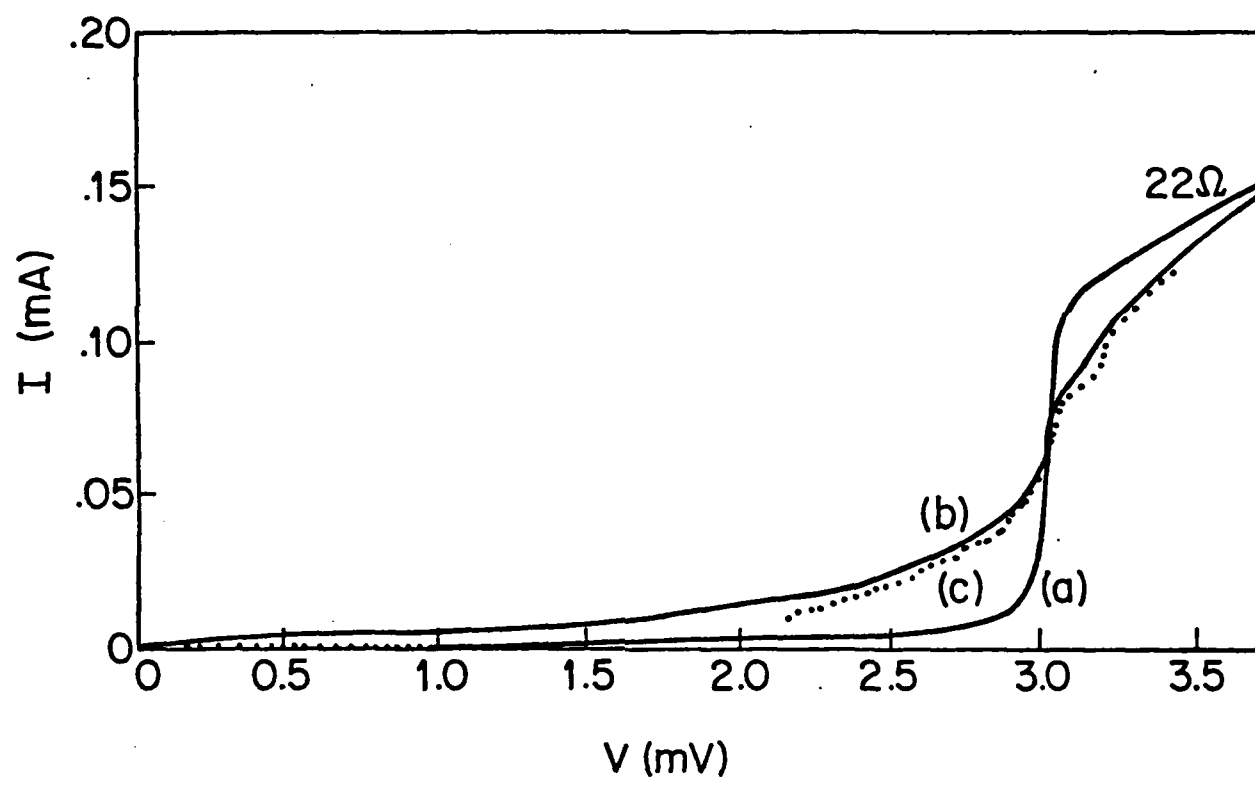
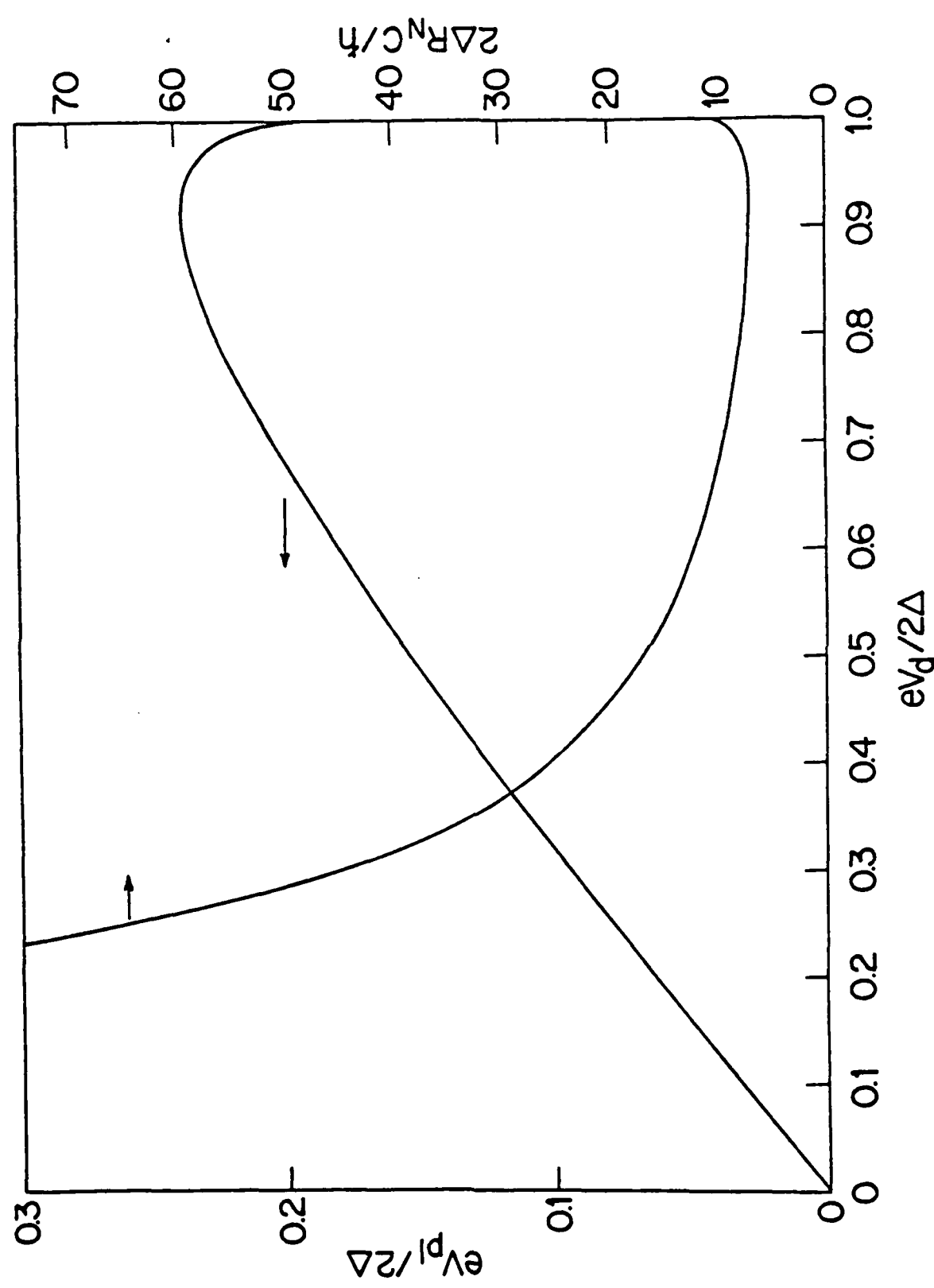


Fig. 7

1000

FIG. 8



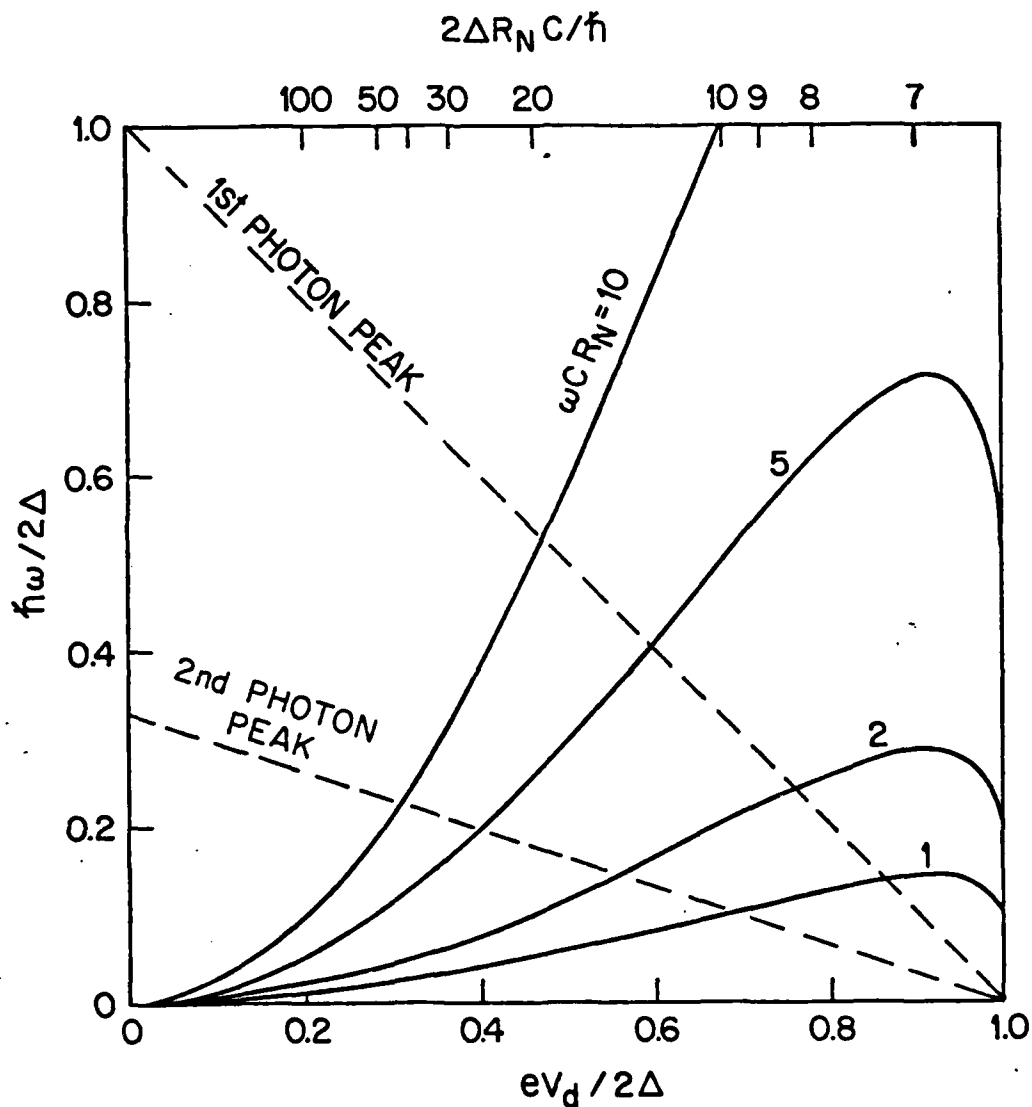


Fig. 9

2010.2.26

